



doi:10.1016/j.gca.2004.03.003

Approaches to surface complexation modeling of Uranium(VI) adsorption on aquifer sediments

JAMES A. DAVIS,^{1,*} DAVID E. MEECE,¹ MATTHIAS KOHLER,^{1,2} and GARY P. CURTIS¹¹U. S. Geological Survey, Menlo Park, CA 94025 USA²Environmental Science and Engineering, Colorado School of Mines, Golden, CO 80401 USA

(Received August 22, 2003; accepted in revised form March 1, 2004)

Abstract—Uranium(VI) adsorption onto aquifer sediments was studied in batch experiments as a function of pH and U(VI) and dissolved carbonate concentrations in artificial groundwater solutions. The sediments were collected from an alluvial aquifer at a location upgradient of contamination from a former uranium mill operation at Naturita, Colorado (USA). The ranges of aqueous chemical conditions used in the U(VI) adsorption experiments (pH 6.9 to 7.9; U(VI) concentration $2.5 \cdot 10^{-8}$ to $1 \cdot 10^{-5}$ M; partial pressure of carbon dioxide gas 0.05 to 6.8%) were based on the spatial variation in chemical conditions observed in 1999–2000 in the Naturita alluvial aquifer. The major minerals in the sediments were quartz, feldspars, and calcite, with minor amounts of magnetite and clay minerals. Quartz grains commonly exhibited coatings that were greater than 10 nm in thickness and composed of an illite-smectite clay with occluded ferrihydrite and goethite nanoparticles. Chemical extractions of quartz grains removed from the sediments were used to estimate the masses of iron and aluminum present in the coatings. Various surface complexation modeling approaches were compared in terms of the ability to describe the U(VI) experimental data and the data requirements for model application to the sediments. Published models for U(VI) adsorption on reference minerals were applied to predict U(VI) adsorption based on assumptions about the sediment surface composition and physical properties (e.g., surface area and electrical double layer). Predictions from these models were highly variable, with results overpredicting or underpredicting the experimental data, depending on the assumptions used to apply the model. Although the models for reference minerals are supported by detailed experimental studies (and in ideal cases, surface spectroscopy), the results suggest that errors are caused in applying the models directly to the sediments by uncertain knowledge of: 1) the proportion and types of surface functional groups available for adsorption in the surface coatings; 2) the electric field at the mineral-water interface; and 3) surface reactions of major ions in the aqueous phase, such as Ca^{2+} , Mg^{2+} , HCO_3^- , SO_4^{2-} , H_4SiO_4 , and organic acids. In contrast, a semi-empirical surface complexation modeling approach can be used to describe the U(VI) experimental data more precisely as a function of aqueous chemical conditions. This approach is useful as a tool to describe the variation in U(VI) retardation as a function of chemical conditions in field-scale reactive transport simulations, and the approach can be used at other field sites. However, the semi-empirical approach is limited by the site-specific nature of the model parameters. Copyright © 2004 Elsevier Ltd

1. INTRODUCTION

Uranium (U) is a contaminant of concern to the U. S. federal government at thousands of sites where it has been released to the environment or where it remains in storage in poorly designed facilities (Crowley and Ahearne, 2002). For example, at U. S. Department of Energy (DOE) facilities, U is the most common radionuclide contaminant in groundwater/sediment systems (Riley et al., 1992). Leaching of U mill tailings has resulted in the contamination of soils and aquifers, with the development of groundwater plumes with high concentrations of dissolved U and other metal ions (Abdelouas et al., 1999). Risk assessments must be conducted for many of these contaminated sites to evaluate remediation and cleanup scenarios, and a significant component of such risk assessments includes predictions of U transport to drinking water supplies or biologic receptors via a groundwater pathway (USEPA, 1999).

Under oxidizing conditions, the most stable valence of U is U(VI) (Grenthe et al., 1992), which is usually present as aqueous carbonate or organic complexes in aquifers (Lenhart et al.,

2000; Davis, 2001; Davis and Curtis, 2003.). U(VI)-bearing minerals are soluble under favorable geochemical conditions, and U(VI) can be very mobile in aquifers (Abdelouas et al., 1999). At circumneutral pH and in the absence of strong complexing agents, U(VI) transport is limited by strong adsorption on mineral surfaces in soils and sediments (Waite et al., 1994; Kohler et al., 1996; Turner et al., 1996; Pabalan et al., 1998; Chisholm-Brause et al., 2001; Prikryl et al., 2001; Barnett et al., 2002; Davis et al., 2002). Subsurface materials with a significant clay content may bind U(VI) by an ion exchange process, but U(VI) is also bound strongly at the edge sites of these minerals by surface complex formation (Turner et al., 1996). Systems where the ion exchange contribution to overall U(VI) adsorption predominates may be limited to those with a specific range of aqueous conditions (low ionic strength, low pH, and low Ca^{2+} concentrations; Turner et al., 1996). Thus, in many contaminated aquifers, U(VI) adsorption is likely dominated by complexation with ionizable hydroxyl sites on oxide mineral surfaces and the edge sites of clay minerals (Pabalan et al., 1998).

Although there is a general consensus that U(VI) transport in groundwater is generally controlled by adsorption, there is disagreement concerning the modeling approach that should be

* Author to whom correspondence should be addressed (jadavis@usgs.gov).

used to describe U(VI) adsorption in reactive transport models. For most metal and radionuclide risk assessments conducted by the U. S. government, reactive transport models utilize the distribution coefficient (constant- K_d) modeling approach to describe the retardation of metal and radionuclide contaminants in aquifers caused by adsorption reactions (USEPA, 1999; Bethke and Brady, 2000). Significant uncertainty in the calculation of retardation may be introduced when the constant- K_d modeling approach is used, due to temporal or spatial variations in groundwater chemistry (Read et al., 1998; Bethke and Brady, 2000; Glynn, 2003). One reason this may occur is because K_d values are very sensitive to chemical conditions. For example, Figure 1 shows the dependence of K_d for U(VI) adsorption on the mineral, ferrihydrite, as a function of pH and the partial pressure of carbon dioxide gas ($p\text{CO}_2$). Note that the K_d value at pH 8 decreases by *four orders of magnitude* as the $p\text{CO}_2$ increases from its value in air to 1%. This is an important variation to understand (Wazne et al., 2003), because the $p\text{CO}_2$ in aquifers commonly reaches values of 1–5% (Hem, 1985), while most K_d values for U(VI) have been determined in laboratory experiments exposed to air (USEPA, 1999). Moreover, $p\text{CO}_2$ often increases with transport after groundwater recharge, and such a spatial/temporal trend in chemical conditions can greatly affect U(VI) transport (Davis and Curtis, 2003).

In contrast to the constant- K_d modeling approach, surface complexation models (SCM) have the capability of describing changes in metal and radionuclide adsorption as chemical conditions and aqueous speciation vary (e.g., Waite et al., 1994; Pabalan et al., 1998; Kohler et al., 1999; Koretsky, 2000; Davis, 2001; Davis et al., 2002). SCM describe the equilibria between aqueous chemical species and species formed at min-

eral surfaces (i.e., surface complexes) through mass action equations, and SCM can be readily incorporated within solute transport models (Kohler et al., 1996; Stollenwerk, 1998; Papini et al., 1999; Kent et al., 2000; Parkhurst et al., 2003; Curtis et al., 2004). The formation of distinct chemical species at mineral surfaces is well accepted in the geochemical literature (e.g., Bargar et al., 2000; Sylwester et al., 2000; Alcacio et al., 2001; Becker et al., 2001; Brown and Parks, 2001; Sverjensky, 2001). Despite their significance, however, surface species have often not been included in geochemical equilibrium or reactive solute transport models because of a poor understanding of the thermodynamics of surface complex formation in natural systems.

There is considerable experimental data for metal ion adsorption (including U(VI)) in systems with one mineral phase, and SCM have been developed to accurately describe these data (e.g., Waite et al., 1994; Pabalan et al., 1998; Arnold et al., 2001). Nevertheless, the application of SCM to the mixtures of minerals in soils and sediments is difficult because of the presence of secondary mineral and organic coatings (Coston et al., 1995; Padmanabhan and Mermut, 1996; Penn et al., 2001; Jove-Colon et al., 2004) that affect the stoichiometry and coulombic correction factors of surface complexation reactions. There are two major approaches for applying the SCM concept to soils and sediments: the Component Additivity (CA) and Generalized Composite (GC) approaches (Davis et al., 1998). In the CA approach, it is assumed that a mineral assemblage is composed of a mixture of one or more reference phases, whose surface chemical reactions are known from independent studies of each phase (e.g., Cowan et al., 1992; Turner et al., 1996; Arnold et al., 2001; Prikryl et al., 2001). Then, based on a measurement of the relative amounts or surface areas of each

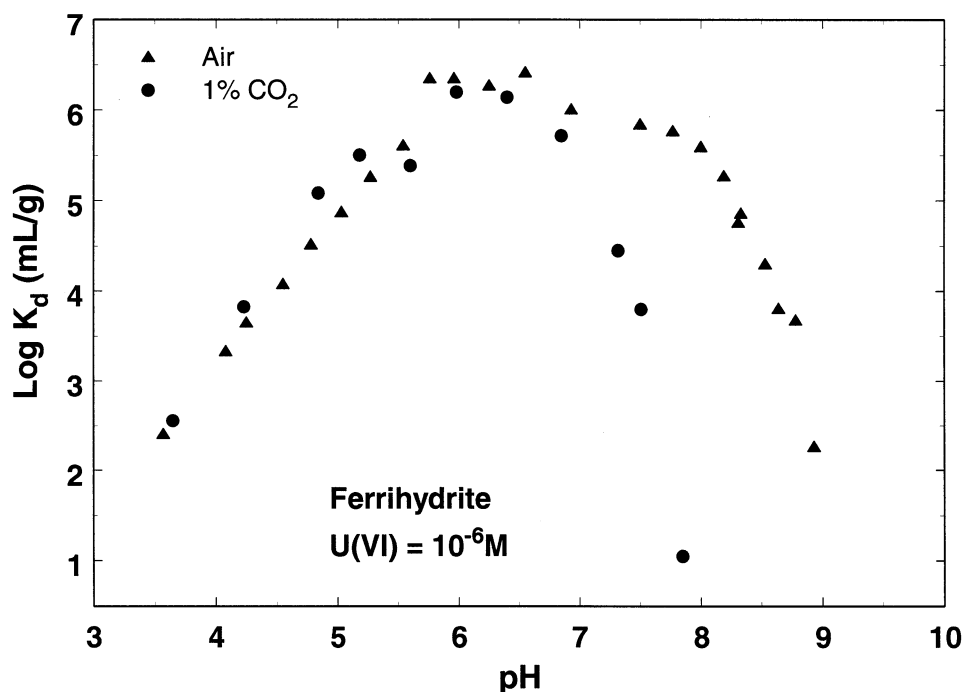


Fig. 1. K_d values for uranium(VI) adsorption on a pure ferrihydrite surface as a function of pH and the partial pressure of carbon dioxide gas (total U(VI) concentration of 10^{-6}M). Points recalculated from the data of Waite et al. (1994).

mineral present in the soil or sediment, adsorption by the mixture of phases can be *predicted* by an equilibrium calculation, without any fitting of experimental data for the mixture (Honeyman, 1984). CA model predictions are sometimes made by assuming that one mineral component dominates adsorption (Davis et al., 1998; Schmeide et al., 2000; Barnett et al., 2002; Waite et al., 2000), allowing a straightforward equilibrium calculation if the exposed surface area of that mineral component in the soil or sediment can be quantified.

In the GC approach, the surface of the mineral assemblage is considered too complex to be quantified in terms of the contributions of individual phases to adsorption. The complexity is caused, in part, by the difficulties in quantifying the electrical field and proportions of surface functional groups at the mineral-water interface in the mixture of mineral phases and associated surface coatings. In the GC approach it is assumed that adsorption can be described by mass laws written with “generic” surface functional groups, with the stoichiometry and formation constants for each mass law determined by fitting experimental data for the mineral assemblage as a whole (van Benschoten et al., 1998; Davis et al., 1998; Westall et al., 1998; Davis et al., 2002).

In this paper, we present GC and CA model calculations to simulate U(VI) adsorption by subsurface sediments collected from the alluvial aquifer at a U mill tailings site near Naturita, Colorado, managed by the DOE UMTRA (Uranium Mill Tailings Remediation Action) program. Together with a series of companion papers (Curtis et al., 2004; Kohler et al., 2004a), it is shown that a simpler, semiempirical model developed with the GC approach can be readily applied to predict *in situ* K_d values or can be incorporated within a reactive transport model for U(VI). The results demonstrate some of the difficulties in employing the CA modeling approach that are caused by mineral coatings in sediments. However, it is also shown that the simpler GC modeling approach can currently be utilized to great advantage in reactive transport modeling to describe adsorption and retardation in aquifers characterized by variable groundwater chemistry.

2. MATERIAL AND METHODS

2.1. Naturita Alluvial Aquifer Sediments

2.1.1. Site description

The Naturita UMTRA site (Fig. 2) is located in the southwestern portion of Colorado in Montrose County, ~3 km northwest of the town of Naturita and on the west bank of the San Miguel River (Davis and Curtis, 2003). From 1947 to 1963, the Naturita mill processed 6.4×10^8 kg of uranium-vanadium ore, using both acid and carbonate leaching to extract uranium and vanadium (USDOE, 1996). Tailings were slurried to the land surface. Uranium contamination in groundwater at the site has been observed primarily within an unconfined, shallow alluvial aquifer composed of sand, gravel, pebbles, and cobbles (Davis and Curtis, 2003). The aquifer is recharged by the San Miguel River at various locations along the reach. The saturated thickness of the alluvial aquifer is ~3 to 4 m.

2.1.2. Preparation of the Naturita aquifer background sediment (NABS) sample

On July 16–17, 1998, approximately 1300 kg of material from the saturated zone of the Naturita alluvial aquifer were collected from a gravel pit located ~90 m upgradient of the site's southern boundary and 40 m from the western edge of the San Miguel River (Fig. 2). The

sample was screened in the field to remove cobbles larger than 64 mm. It was visually estimated that 50% of the material scooped by the backhoe did not pass the 64 mm screen. Groundwater at this location was mildly reducing, with very low concentrations of both dissolved oxygen and Fe^{2+} (Davis and Curtis, 2003).

Wet sediments (734 kg, <64 mm) were shipped in clean plastic containers to the USGS laboratories in Menlo Park, California, and the sediments were air dried on plastic sheets (dry weight = 641 kg). The sediments were sieved to separate grains <3 mm from coarser material. 190 kg of sediments passed the 3 mm screen, representing roughly 30% (by weight) of the <64 mm material collected in the field. The 190 kg of <3 mm sediments was thoroughly mixed and is referred to as the Naturita aquifer background sediment (NABS) sample.

2.2. Characterization of Naturita Sediments

Characterization of the NABS sample that is relevant to this paper is presented here. More details and characterization data are presented in Davis and Curtis (2003) and Kohler et al. (2004a).

The grain size distribution of the NABS sample was determined by wet sieving using 1000, 500, 250, 125, and 63 micron (μm) sieves. Because of the presence of carbonate minerals, an artificial groundwater (AGW) was prepared for sieving that was slightly undersaturated with respect to calcite (ion activity product 0.3 log units less than saturation) and had an ionic strength similar to that of groundwater in the Naturita alluvial aquifer. About 20% of the >3 mm gravel particles, removed during production of the NABS (<3 mm) sample, was dry sieved using 5.613 mm, 9.423 mm, and 16 mm mesh screens. An additional size fraction of the coarsest material was produced by hand picking pebbles of ~30 mm average dimension and larger, up to the 64 mm maximum allowed by the field screening. Specific surface areas of the NABS sample and grain size fractions were determined by BET single-point nitrogen gas adsorption using the flow-through method on a Micromeritics FlowSorb II (Model 2300).

The NABS sample and its grain size fractions were examined by optical and field-emission SEM (FE-SEM). Grains were mounted to an aluminum stub with double-sided tape and examined uncoated. The SEM results were coupled with energy dispersive spectroscopy (EDS) to give compositional information at particular surface locations. Thin sections were coated with Au-Pd to prevent the sample from beam damage during the collection of EDS data.

The labile fraction of U(VI) in the NABS sample and grain size fractions was estimated by the alkaline sodium (bi)carbonate extraction method of Kohler et al. (2004a). The labile fraction is the portion of U(VI) associated with the solid sample that equilibrates on short-time scales with dissolved U(VI) in solutions similar in composition to the Naturita groundwater (Kohler et al., 2004a). In the extraction, adsorbed U(VI) is completely desorbed from the sample by aqueous complexation with carbonate at alkaline pH conditions, and it is believed that adsorbed U(VI) dominates the labile fraction on the NABS sample. The extracting solution contained $1.44 \cdot 10^{-2}$ M NaHCO_3 and $2.8 \cdot 10^{-3}$ M Na_2CO_3 , with the pH adjusted to 9.45. The extractions were carried out at room temperature for a period of 3 weeks.

2.3. Batch U(VI) Adsorption Experiments with Naturita Sediments

Experiments were carried out at five different $p\text{CO}_2$ values to determine the distribution of U(VI) between the NABS sample and artificial groundwater solutions as a function of U(VI) concentration. The experiments were designed partly to simulate chemical conditions in the Naturita alluvial aquifer, with minimal dissolution or precipitation of calcite and with as little alteration of the sediment surfaces as possible. To this end, artificial groundwater solutions were pre-equilibrated with the NABS sediments before use in adsorption experiments (Davis and Curtis, 2003).

2.3.1. Artificial groundwater solutions

Four artificial groundwater solutions (AGWs) were designed so as to approximate the major chemistry of Naturita groundwaters at various $p\text{CO}_2$ (Table 1). To prepare for use in adsorption experiments, the solutions were placed in contact with NABS sediment in stirred flasks

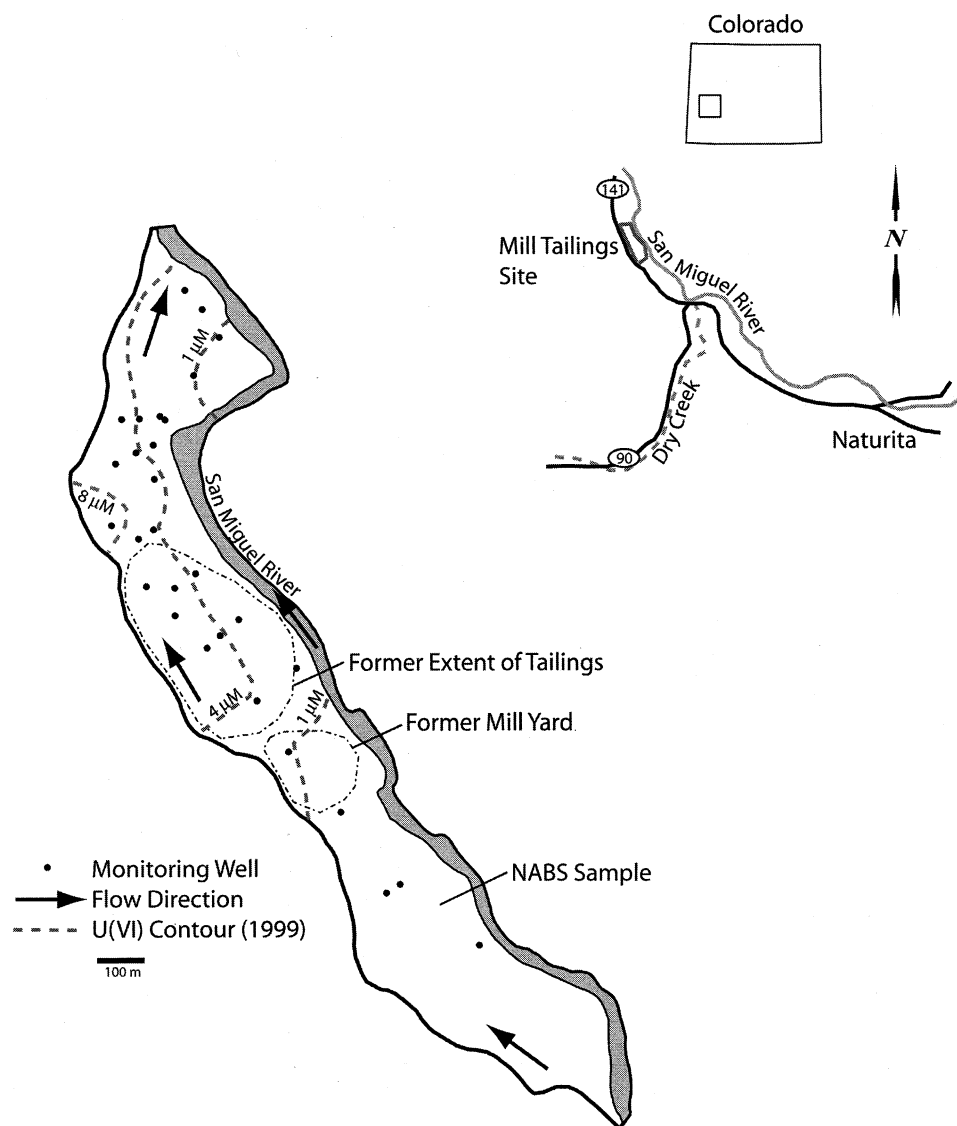


Fig. 2. Locality map showing the Naturita, Colorado, UMTRA site, the location where the NABS sediment sample was collected, the groundwater flow direction, the location of groundwater monitoring wells, and contours for dissolved U(VI) concentrations in the groundwater.

for at least 72 h. 'Certified standard' grade mixed gas of appropriate CO_2 content (balance air) was bubbled through the AGWs using a sparger. Sediments were separated from the preequilibrated solutions by filtration ($0.4 \mu\text{m}$). The composition of the AGW solutions changed only slightly during preequilibration with the sediments, with the largest change being that some dissolved Si was present (e.g., $6 \cdot 10^{-5}$ M in preequilibrated AGW-3, see Davis and Curtis, 2003).

For adsorption experiments, uranium (1000 mg/L, in 2% HNO_3) was added to pretreated AGW to yield a secondary stock solution of 10^{-5} M U(VI). An equivalent amount of NaOH was also added to neutralize the acid in the primary uranium stock solution. Other concentrations of U(VI) were obtained by dilution of the secondary stock solution. Solutions were allowed to sit overnight to allow aqueous U(VI) speciation to approach equilibrium.

2.3.2. Pretreatment of NABS sediments

Two replicate weighed aliquots of NABS sediment (same amount as in U(VI) adsorption experiments, see below) were placed into 50 mL polycarbonate centrifuge tubes in a controlled $p\text{CO}_2$ atmosphere within

Table 1. Composition of artificial groundwater solutions (in moles/L) for U(VI) adsorption experiments.

Name	AGW-3	AGW-7	AGW-5	AGW-6
Initial $p\text{CO}_2$	0.035%	0.5%	2%	10%
	(lab air)			
CaSO_4	$2.33 \cdot 10^{-3}$	$2.32 \cdot 10^{-3}$	$3.27 \cdot 10^{-3}$	$3.27 \cdot 10^{-3}$
MgSO_4	$1.52 \cdot 10^{-3}$	$1.52 \cdot 10^{-3}$	$1.52 \cdot 10^{-3}$	$1.52 \cdot 10^{-3}$
Na_2SO_4	$9.38 \cdot 10^{-4}$	0	0	0
CaCl_2	$2.38 \cdot 10^{-3}$	$3.95 \cdot 10^{-5}$	$2.22 \cdot 10^{-3}$	0
KCl	$6.40 \cdot 10^{-5}$	$6.40 \cdot 10^{-5}$	$6.40 \cdot 10^{-5}$	$6.40 \cdot 10^{-5}$
NaHCO_3	$5.38 \cdot 10^{-4}$	$2.41 \cdot 10^{-3}$	$2.41 \cdot 10^{-3}$	$2.41 \cdot 10^{-3}$
CaCO_3	0	$8.70 \cdot 10^{-5}$	$9.27 \cdot 10^{-4}$	$3.33 \cdot 10^{-3}$
HCl	0	$8.70 \cdot 10^{-5}$	$9.27 \cdot 10^{-4}$	$1.57 \cdot 10^{-3}$
Initial ionic strength ^a	0.0212	0.0152	0.0255	0.0289

^a Calculated with the equilibrium aqueous speciation code HYDRAQL (Papelis et al., 1988).

a glove bag or open to laboratory air. 30 mL of preequilibrated artificial groundwater solution (without added U(VI)) was added to each tube. The tubes were placed on an end-over-end rotator (14 rpm) overnight to preequilibrate the sediment surfaces. The following day the test tubes were centrifuged (25600 g for 20 min) and the supernatant was removed and sampled for pH, alkalinity, and the dissolved background U(VI) concentration. Samples were analyzed by kinetic phosphorescence analysis (KPA) for dissolved U(VI). Alkalinity was measured in filtered (0.45 μm) supernatant by titration with 0.01M HCl.

2.3.3. U(VI) Adsorption experiments

Weighed aliquots of U(VI)-bearing AGW were added to each of the pretreated NABS samples, plus to one empty (control) test tube, which were then capped and returned to the end-over-end rotator. After 96 h the test tubes were centrifuged and the supernatant was sampled for pH, U(VI), and alkalinity. Experimental conditions in the batch adsorption experiments are summarized in Table 2. Because the experimental systems were closed to the atmosphere, the alkalinity and pH evolved slightly during equilibration due to mineral weathering. As a result, the final $p\text{CO}_2$ in the small head space of the centrifuge tube would be expected to be different from that the AGW solutions were initially equilibrated with. Table 2 shows the final $p\text{CO}_2$ concentrations, calculated from the measured pH and alkalinity values.

2.3.4. Calculations

Calculation of U(VI) distributions in the adsorption experiments followed a straightforward mass balance approach. In each case, for each sample test tube, the mass of NABS sediment added was measured and the background labile (exchangeable) U(VI) content of the sediment ($5.6 \pm 0.45 \cdot 10^{-10}$ moles/g) was known from the isotopic exchange studies of Kohler et al. (2004a). The initial and final dissolved U(VI) concentrations in the NABS pretreatment solutions were measured, allowing a calculation of the U(VI) contributed by the residual amount of pretreatment solution before the introduction of U(VI)-spiked AGW solution. U(VI) adsorption on the NABS sample was calculated by difference from the total labile U(VI) present in the experiment minus the dissolved U(VI) present after the 96-h adsorption period.

The background labile U(VI) value determined by the isotopic exchange method was somewhat lower than that determined for the NABS sediment by the carbonate extraction method ($8.74 \pm 0.44 \cdot 10^{-10}$ moles/g, Table 3, see discussion below). At the higher U(VI) concentrations present in contaminated sediments at Naturita, the carbonate extraction and isotopic exchange methods provide very similar estimates of labile U(VI) content (Kohler et al., 2004a). At the very low U(VI) concentrations in the background NABS sample, however, the isotopic exchange method yields a smaller value for labile U(VI) than the carbonate extraction method. Because the isotopic exchange method involves chemical conditions more similar to those in the batch adsorption experiments, the isotopic exchange method was used to estimate the labile U(VI) that was added to the experiments as background U(VI). The background U(VI) was only significant in the mass balance calculations for the experiments conducted at the lowest U(VI) concentrations.

Table 2. Final chemical conditions in U(VI) adsorption experiments.

Initial $p\text{CO}_2$	AGW solution	Solid/liquid Ratio (g/L)	Average final pH	Average final alkalinity (meq/L)	Final $p\text{CO}_2^a$
Lab air	AGW-3	25	7.94	0.75	0.05%
0.5%	AGW-7	125	7.58	3.05	0.47%
2%	AGW-5	125	7.22	3.58	1.24%
2%	AGW-5	250	7.18	4.04	1.57%
10%	AGW-6	820	6.88	9.13	6.8%

^a Calculated from the average measured final pH and alkalinity.

Table 3. Grain size distribution, surface area, and labile U(VI) of the NABS^a sample and size fractions.

Sample	Weight %	Surface Area (m ² /g)	Labile U(VI) (mol/g)	Labile U(VI) (mol/m ²)	% of Labile U(VI)
NABS	29.7 ^b	5.15	$8.74 \cdot 10^{-10}$	$1.69 \cdot 10^{-10}$	83.6 ^c
Size fractions					
<63 μm	1.1	13.1	$2.50 \cdot 10^{-9}$	$1.91 \cdot 10^{-10}$	11.5
63–125 μm	1.9	7.19	$1.06 \cdot 10^{-9}$	$1.47 \cdot 10^{-10}$	8.4
125–250 μm	4.9	5.1	$6.36 \cdot 10^{-10}$	$1.25 \cdot 10^{-10}$	13
250–500 μm	6.8	3.95	$4.79 \cdot 10^{-10}$	$1.21 \cdot 10^{-10}$	13.6
0.5–1 mm	4.7	5.7	$5.36 \cdot 10^{-10}$	$0.94 \cdot 10^{-10}$	10.5
1–3 mm	10.1	6.31	$6.26 \cdot 10^{-10}$	$0.99 \cdot 10^{-10}$	26.4
3–5.6 mm	7.8	3.57	$1.28 \cdot 10^{-10}$	$0.36 \cdot 10^{-10}$	4.2
5.6–9.4 mm	10.1	3.33	$8.54 \cdot 10^{-11}$	$0.26 \cdot 10^{-10}$	3.6
9.4–16 mm	12.8	na ^d	$7.03 \cdot 10^{-11}$	na	3.8
16–30 mm	17.6	na	$3.44 \cdot 10^{-11}$	na	2.5
30–64 mm	22.0	na	$2.57 \cdot 10^{-11}$	na	2.4

^a Naturita aquifer background sediment (<3 mm).

^b <3 mm sample was 29.7% of the <64 mm sediments.

^c <3 mm sample had 83.6% of the sum of labile U(VI) in sediments <64 mm.

^d not analyzed.

2.4. Modeling

FITEQL 4.0 (Herbelin and Westall, 1999) was used to determine the best fit of various U(VI) surface reactions or combinations of reactions to the experimental U(VI) adsorption data in the Generalized Composite model calculations. The Davies equation was used for activity correction of aqueous species only. Relative errors of 1% in the concentrations of surface sites, total U(VI), and adsorbed U(VI), and relative errors of 5% in $\log [\text{H}^+]$ and $\log [\text{H}_2\text{CO}_3]$ were used as FITEQL inputs. Thermodynamic data used in the modeling are given in Table 4 and are generally consistent with the NEA database for uranium (Grenthe et al., 1992; Silva et al., 1995), except that the aqueous species, $\text{CaUO}_2(\text{CO}_3)_2^{2-}$ and $\text{Ca}_2\text{UO}_2(\text{CO}_3)_2^0(\text{aq})$ (Kalmykov and Choppin, 2000; Bernhard et al., 2001), were also considered here. Recent results (Brooks et al., 2003) confirm the existence of these species, and aqueous speciation calculations with the thermodynamic data of Bernhard et al. (2001) and Kalmykov and Choppin (2000) suggest that these species are the predominant aqueous species in Naturita groundwaters (96–98% of dissolved U(VI)) and for U(VI) in groundwaters at other UMTRA sites (Brooks et al., 2003).

3. RESULTS

3.1. Grain Size, Surface Area, and Background U Distributions of the Naturita Sediments

Table 3 shows the grain size distribution of the NABS sample, surface area measurements, and the amount of labile U(VI), as determined by the carbonate extraction method (Kohler et al., 2004a). In general, the amount of material in each size fraction increased with particle size, with gravels coarser than 3 mm comprising $\sim 70\%$ of the total mass of the <64 mm sample (Davis and Curtis, 2003). The <3 mm material, which was used to prepare a large composite sample (NABS) for characterization and the U(VI) adsorption experiments, comprised 30% of the mass <64 mm.

Overall, the sediments were composed of poorly sorted, weathered and abraded rocks of many varieties. Minerals in the NABS sample are mostly quartz with lesser amounts of detrital feldspars, carbonates, magnetite, and clay minerals. The clay fraction is highly variable, ranging mostly from intricate mixed

Table 4. Formation constants for U(VI) solution species.

Reaction	$\log \beta^*$ ($I = 0$) ^a
$\text{UO}_2^{2+} + \text{H}_2\text{O} \rightleftharpoons \text{UO}_2\text{OH}^+ + \text{H}^+$	-5.20
$\text{UO}_2^{2+} + 2\text{H}_2\text{O} \rightleftharpoons \text{UO}_2(\text{OH})_2(\text{aq}) + 2\text{H}^+$	-11.50 ^b
$\text{UO}_2^{2+} + 3\text{H}_2\text{O} \rightleftharpoons \text{UO}_2(\text{OH})_3^{2-} + 3\text{H}^+$	-20.00 ^c
$\text{UO}_2^{2+} + 4\text{H}_2\text{O} \rightleftharpoons \text{UO}_2(\text{OH})_4^{2-} + 4\text{H}^+$	-33.0
$2\text{UO}_2^{2+} + \text{H}_2\text{O} \rightleftharpoons (\text{UO}_2)_2\text{OH}^{3+} + \text{H}^+$	-2.70
$2\text{UO}_2^{2+} + 2\text{H}_2\text{O} \rightleftharpoons (\text{UO}_2)_2(\text{OH})_2^{2+} + 2\text{H}^+$	-5.62
$3\text{UO}_2^{2+} + 4\text{H}_2\text{O} \rightleftharpoons (\text{UO}_2)_3(\text{OH})_4^{2+} + 4\text{H}^+$	-11.90
$3\text{UO}_2^{2+} + 5\text{H}_2\text{O} \rightleftharpoons (\text{UO}_2)_3(\text{OH})_5^{2+} + 5\text{H}^+$	-15.55
$3\text{UO}_2^{2+} + 7\text{H}_2\text{O} \rightleftharpoons (\text{UO}_2)_3(\text{OH})_7^{2+} + 7\text{H}^+$	-31.00
$4\text{UO}_2^{2+} + 7\text{H}_2\text{O} \rightleftharpoons (\text{UO}_2)_4(\text{OH})_7^{2+} + 7\text{H}^+$	-21.9
$\text{UO}_2^{2+} + \text{CO}_3^{2-} \rightleftharpoons \text{UO}_2\text{CO}_3(\text{aq})$	9.67 ^d
$\text{UO}_2^{2+} + 2\text{CO}_3^{2-} \rightleftharpoons \text{UO}_2(\text{CO}_3)_2^{2-}$	16.94
$\text{UO}_2^{2+} + 3\text{CO}_3^{2-} \rightleftharpoons \text{UO}_2(\text{CO}_3)_3^{4-}$	21.60
$3\text{UO}_2^{2+} + 6\text{CO}_3^{2-} \rightleftharpoons (\text{UO}_2)_3(\text{CO}_3)_6^{6-}$	54.0
$2\text{UO}_2^{2+} + \text{CO}_3^{2-} + 3\text{H}_2\text{O} \rightleftharpoons (\text{UO}_2)_2\text{CO}_3(\text{OH})_3^{-} + 3\text{H}^+$	-0.86
$3\text{UO}_2^{2+} + \text{CO}_3^{2-} + 3\text{H}_2\text{O} \rightleftharpoons (\text{UO}_2)_3\text{CO}_3(\text{OH})_3^{+} + 3\text{H}^+$	0.66
$\text{UO}_2^{2+} + \text{Cl}^- \rightleftharpoons \text{UO}_2\text{Cl}^+$	0.17
$\text{Ca}^{2+} + \text{UO}_2^{2+} + 3\text{CO}_3^{2-} \rightleftharpoons \text{CaUO}_2(\text{CO}_3)_3^{2-}$	25.4 ^e
$2\text{Ca}^{2+} + \text{UO}_2^{2+} + 3\text{CO}_3^{2-} \rightleftharpoons \text{Ca}_2\text{UO}_2(\text{CO}_3)_3(\text{aq})$	30.55 ^e
$\text{UO}_2^{2+} + 2\text{Cl}^- \rightleftharpoons \text{UO}_2\text{Cl}_2(\text{aq})$	-1.1
$\text{UO}_2^{2+} + \text{SO}_4^{2-} \rightleftharpoons \text{UO}_2\text{SO}_4(\text{aq})$	3.15
$\text{UO}_2^{2+} + 2\text{SO}_4^{2-} \rightleftharpoons \text{UO}_2(\text{SO}_4)_2^{2-}$	4.14
$\text{UO}_2^{2+} + \text{SiO}_2(\text{OH})_2^{2-} + \text{H}^+ \rightleftharpoons \text{UO}_2\text{SiO}(\text{OH})_3^{+}$	21.54 ^f

^a Values from Grenthe et al. (1992), unless otherwise indicated.

^b Silva (1992), $\log K = -11.5$ was used, reference gives $\log K \leq -11.5$.

^c Sandino and Bruno (1992).

^d Silva et al. (1995).

^e Bernhard et al. (2001).

^f Moll (1997).

layer illite/smectite clays to the minor presence of chlorite (Jove-Colon et al., 2004). According to Sanpawanitchakit (2002), the NABS sample is 36.6% Si, 3.97% Al, and 2.77% Fe by weight. The total carbon content of the sample was 0.36% by weight, with 0.25% as inorganic carbon and 0.11% as organic carbon. Extractions with an acetic acid buffer (pH 5) suggest that carbonate minerals were 2.5% by weight of the sample with an average composition of $(\text{Ca}_{0.92}\text{Mg}_{0.08})\text{CO}_3$ (Sanpawanitchakit, 2002).

Specific surface areas were determined by BET for the size fractions up to 9.4 mm (Table 3). The finest material had the highest surface area (13.11 m²/g), and the surface areas of the remaining fractions were surprisingly high and relatively consistent. Instead of decreasing rapidly as grain size increased, the surface areas decreased to a local minimum of 3.95 m²/g for the 250–500 μm fraction, increased to 6.31 m²/g for the 1.0–3.0 mm fraction, and the decreased again to 3.33 m²/g for the coarsest fraction measured (5.6–9.4 mm).

Under optical microscopic examination, the 1–3 and 0.5–1 mm fractions appeared to be composed largely of aggregates and polycrystalline lithic fragments of many types, as opposed to single crystalline grains. Grains in the 250–500 and 125–250 μm size fractions that contained the surface area minimum were primarily discrete, clean, rounded quartz sand grains, similar to the one in the aggregate described above. Quartz predominated in the two finest fractions (63–125 and <63 μm) as well, with a smaller amount of platy material, likely clays, visible at highest magnification. Calcite was generally not

present as cement but as individual crystals or clusters of disseminated crystals, usually between 2 and 10 μm in size.

The most common surface morphology observed was a rougher texture of angular platy shapes (Fig. 3), suggestive of clay mineralogy (EDS spectral analysis indicated K, Al, and Si). The coating appeared to cement grains together into aggregates. The extremely textured and porous surfaces of the larger grains strongly resembled the textures of the <63 μm fraction, which may explain the relatively high surface areas

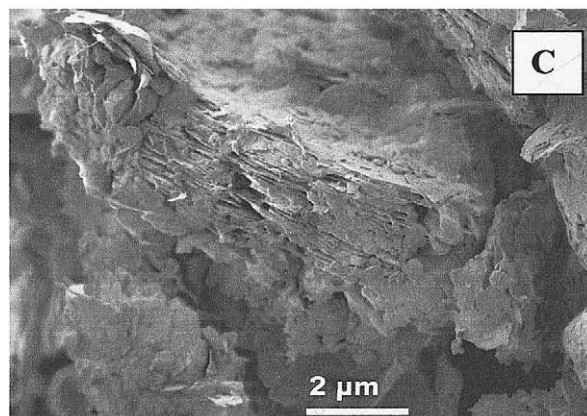
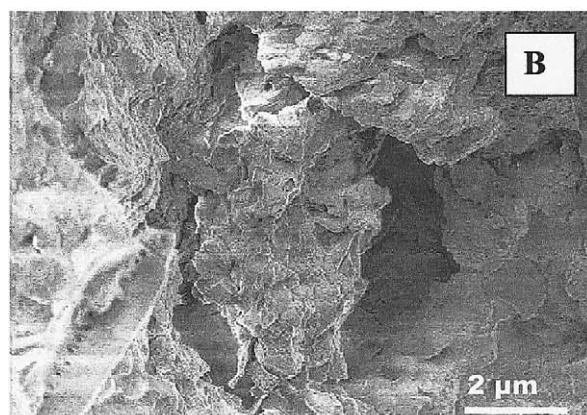
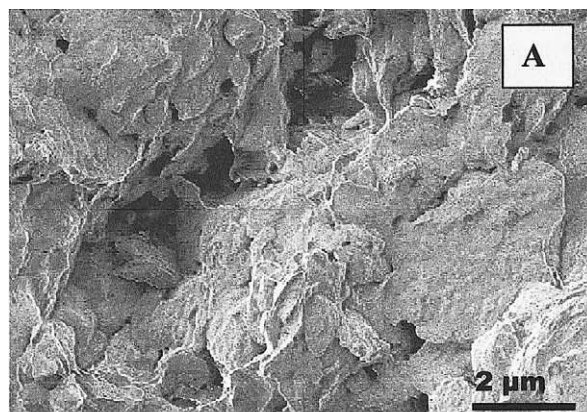


Fig. 3. Field Emission SEM images of two grain size fraction samples prepared from the NABS sample. All grain size fractions examined had an adhered clay mineral coating covering the underlying mineral grains. For example, image A is from the <63 μm fraction while images B and C are from grains greater than 500 μm in diameter.

measured for the 500–1000 μm and 1–3 mm size fractions. This conclusion was further substantiated by SEM examination of thin sections: the majority of large grains had exterior coatings of adhered fine-grained minerals tens of microns thick. Using a variety of advanced characterization methods (electron microscopy and secondary ion mass spectroscopy), Jove-Colon et al. (2004) found that all grains examined exhibited Fe-rich and Al-Si-rich coatings (Fig. 4). The Fe-rich coatings were

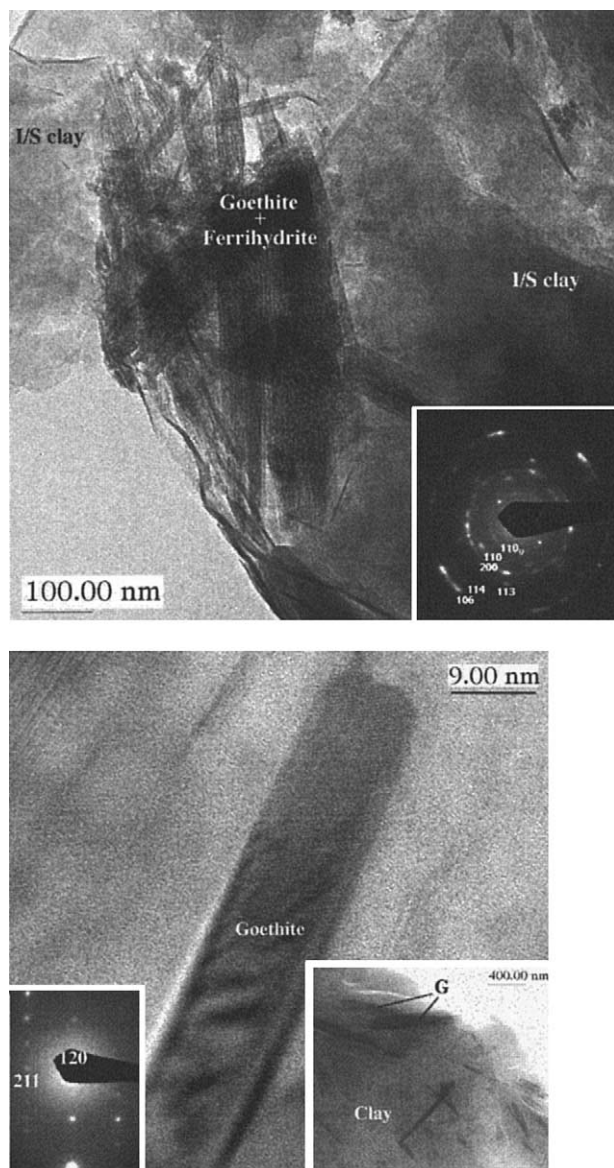


Fig. 4. **a)** Low-magnification, bright-field TEM image of a Naturita grain coating showing plate-like goethite with some ferrihydrite immersed in illite-smectite clay, denoted as I/S clay in figure (Jove-Colon et al., 2004). The lower right corner shows a weak electron diffraction pattern labeled as 110g, indicating a small amount of goethite mixed with a predominant ferrihydrite phase. **b)** Bright-field TEM images of the same grain coating as 4a), showing needle-like goethite crystals immersed in illite-smectite clay, labeled as clay in figure (Jove-Colon et al., 2004). Inserted is a selected area electron diffraction pattern (left corner) of the goethite crystal at the center of the high magnification image. Low-magnification TEM image showing many goethite needles (G) in the coating (right corner).

arranged conformably in both continuous and discontinuous modes, in some cases between the quartz interface and clay-rich coating. However, Fe-rich phases were also present as small scattered particles immersed in the clay coatings (Fig. 4). The Fe-bearing phases were highly heterogeneous, composed mainly of mixed domains of hematite, goethite, and amorphous iron oxyhydroxides (Jove-Colon et al., 2004).

Table 3 shows the concentrations of labile U(VI) for the NABS sample and its size fractions estimated by the carbonate extraction method. Total U in the NABS sample, which includes U in crystalline phases, is $9.64 \cdot 10^{-9}$ moles/g (Kohler et al., 2004a), and thus, the labile U(VI) is estimated at $\sim 9\%$ of the total U. In contrast, U-contaminated sediments collected at the Naturita site had much higher fractions of labile U(VI) (Kohler et al., 2004a). This is consistent with the hypothesis that the labile fraction is present primarily as U(VI) adsorbed on the mineral surfaces. Per unit weight, the fine size fractions contained the greatest concentrations of labile U(VI); however, the larger size fractions also contained significant amounts of labile U(VI). When normalized to surface area, the concentrations of labile U(VI) were surprisingly similar among the grain size fractions < 3 mm. This suggests that mineral coatings likely play a major role in the adsorption of U(VI), and the ubiquitous presence and similarity of the coatings among the size fractions (Fig. 3) results in little differentiation in U(VI) adsorption among the grain size fractions less than 3 mm diameter.

Although the NABS < 3 mm sample comprised only $\sim 30\%$ of the sediments < 64 mm, it contained $\sim 84\%$ of the labile U(VI) (Table 3). A considerable fraction of the labile U(VI) was present in the 1–3 mm size fraction, possibly because many grains in this size range appeared to be cemented aggregates of smaller grains with significant porosity. The fact that a large fraction of the labile U(VI) was present in the NABS < 3 mm composite sample suggests that the sample should provide a good representation of U(VI) adsorption reactions within the Naturita alluvial aquifer.

3.2. U(VI) Batch Adsorption Experiments with the NABS Sample

Kinetic experiments were carried out to determine the length of time necessary to achieve steady state solution concentrations of U(VI) in an artificial groundwater solution (AGW-3) in contact with the NABS sample or its grain size fractions. These experiments were carried out with 10^{-6} M U(VI) added to AGW-3 solution at equilibrium with atmospheric CO_2 . Under these conditions, the AGW-3 solution had an equilibrium pH of 7.94 ± 0.05 (Table 2).

The results of these experiments are presented as K_d and K_a values in Figure 5. Because the samples are of unequal surface area, the results are best compared with a surface-area distribution coefficient, $K_a = K_d/A$, where A is the specific surface area in m^2/g . The results show that U(VI) adsorption continued to approach adsorptive equilibrium for at least 96 h. The fine grain size fractions adsorbed more U(VI) per unit mass than the coarse fractions (Fig. 5A), but

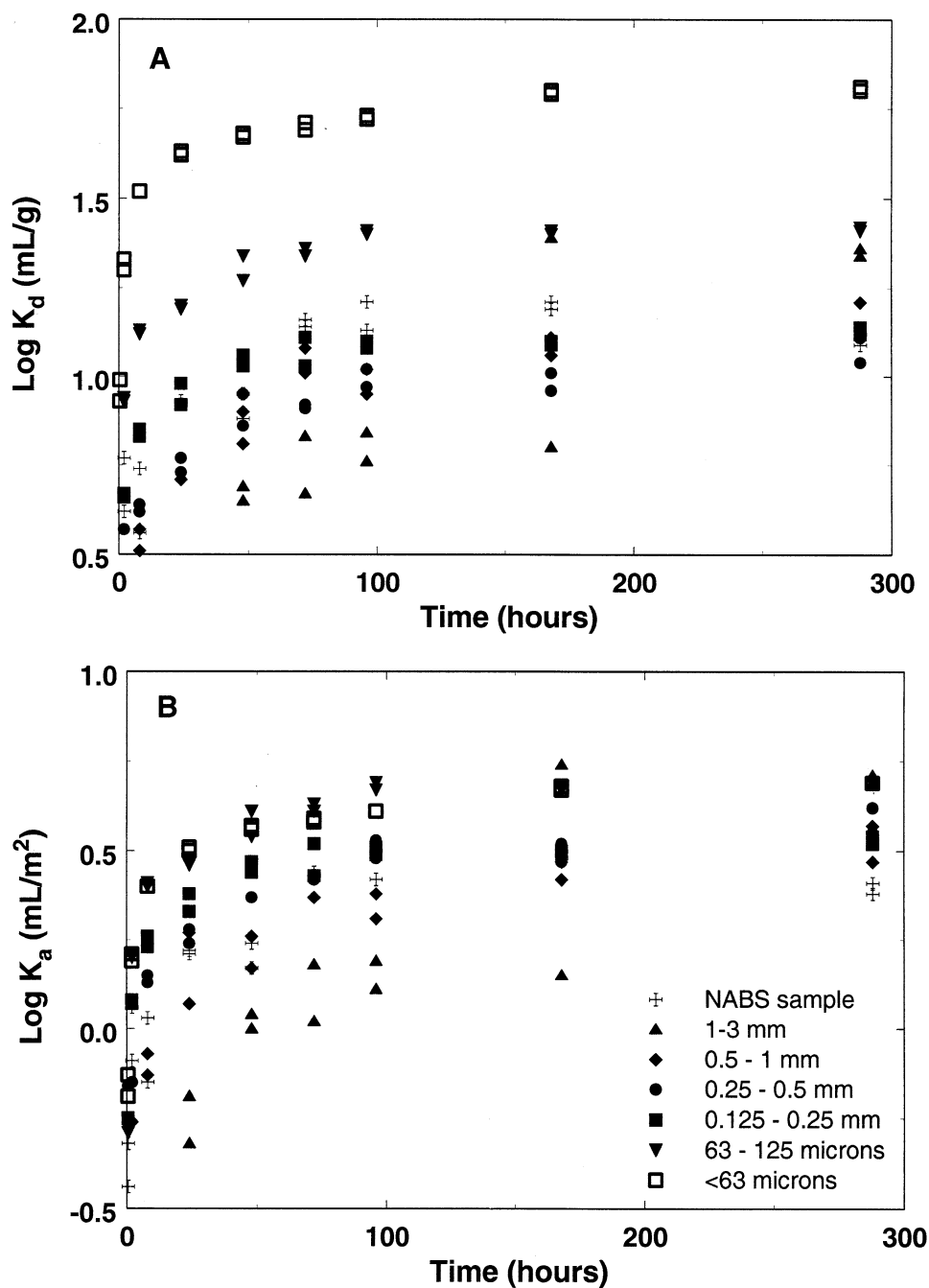


Fig. 5. Kinetics of U(VI) adsorption by the NABS sample and grain size fractions in AGW-3 solutions equilibrated with air, containing 25 g/L of sediment and with 10^{-6} M U(VI) added to the experiment at time = 0; pH = 7.94. Part A) plotted as K_d (mL/g), and Part B) plotted as K_a (mL/m²). Symbols are the same in Part A) and B).

some of this difference was eliminated by accounting for surface area differences (Fig. 5B). The approach to U(VI) adsorptive equilibrium was slower with the larger grain sizes, perhaps due to the porosity observed in the grains.

Batch adsorption isotherm experiments with the NABS sample were conducted with reaction times of 96 h, which allowed enough time to approach steady-state dissolved U(VI) concentrations (Fig. 5). The pH in each set of experiments approached a unique value that was dependent on the

solid/liquid ratio and artificial groundwater composition (Table 2). Total U(VI) added to the experiments varied from zero (in which the desorption of background labile U(VI) was evaluated, Kohler et al., 2004a) to 1×10^{-5} M. Figure 6a shows fractional adsorption of U(VI) on NABS as a function of the U(VI) concentration, $p\text{CO}_2$, and pH. The aqueous conditions at the highest $p\text{CO}_2$ (6.8%) approach those observed in the Naturita alluvial aquifer (Davis and Curtis, 2003). Fractional adsorption decreased as the U(VI)

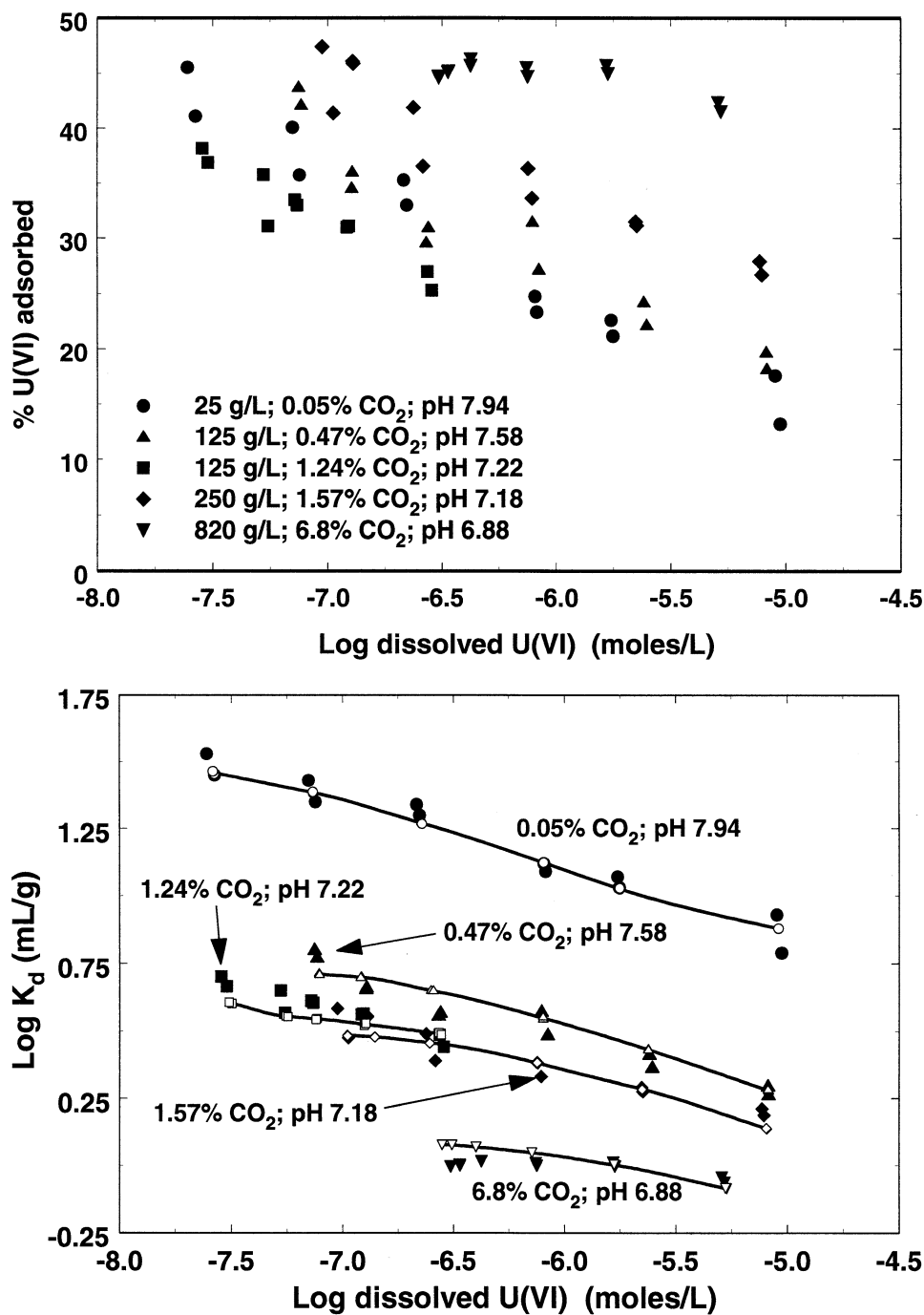


Fig. 6. a) Fractional U(VI) adsorption on the <3mm NABS composite sample as a function of the partial pressure of carbon dioxide, pH, and solid/liquid ratio. Reaction time of 96 h. b) U(VI) adsorption on the <3mm NABS composite sample as a function of the partial pressure of carbon dioxide, pH, and solid/liquid ratio expressed as $\log K_d$ values. Experimental data points (shown as solid symbols) are the same as in Figure 6a. Generalized Composite SCM simulations are shown as smoothed solid curves drawn through the open symbols.

concentration increased, as has been observed for quartz, aluminosilicate minerals, and iron oxides (Waite et al., 1994; Davis, 2001). Adsorption also decreased as the $p\text{CO}_2$ increased, but the decrease is not obvious in Figure 6a because the solid/liquid ratio in the experiments was increased simultaneously. When plotted as the log of the U(VI) adsorp-

tion density versus the log of the dissolved U(VI) concentration (not shown), the adsorption isotherms have a slope of 0.75, consistent with isotherms determined for U(VI) on pure quartz (Kohler et al., 1996; Davis, 2001). Figure 6b shows the same experimental data plotted as $\log K_d$ values versus the log of the dissolved U(VI) concentration.

3.3. Mineral Component and Component Additivity SCM Predictions

To carry out transport simulations of uranium transport in the Naturita aquifer (Davis and Curtis, 2003; Curtis et al., 2004), a surface complexation model is needed to describe the adsorption of U(VI) on the aquifer sediments. Two types of surface complexation modeling were tested for this purpose: 1) Predictions of U(VI) adsorption on mineral components of the Naturita sediments from models developed for single mineral phases in simple electrolyte solutions; and 2) Development of a semiempirical model, fit to the U(VI) adsorption data on the sediments, using the Generalized Composite modeling approach (Davis et al., 1998; Davis et al., 2002). In both cases, the formation constants for U(VI) aqueous species given in Table 4 were used in the calculations. It is important to note that the species, $\text{CaUO}_2(\text{CO}_3)_3^{2-}$ and $\text{Ca}_2\text{UO}_2(\text{CO}_3)_3^0(\text{aq})$ (Kalmykov and Choppin, 2000; Bernhard et al., 2001; Brooks et al., 2003), dominated the

calculated speciation for dissolved U(VI). For the range of chemical conditions considered in the batch experiments, these two species accounted for 96.3–98.8% of dissolved U(VI). These species are not yet included in many thermodynamic databases for uranium; for comparison, alternative SCM calculations without these species are available in Davis and Curtis (2003).

Since quartz constitutes the bulk of the Naturita sediments by weight, the first step in building a Component Additivity model was to consider U(VI) adsorption reactions with silanol functional groups. Kohler et al. (2004b) developed a triple-layer model (TLM) to describe U(VI) adsorption on quartz in NaNO_3 solution as a function of pH, U(VI) concentration, and the partial pressure of CO_2 . The parameters for the quartz model are given in Table 5. Strong- and weak-binding sites are typically defined in such models to describe adsorption data as a function of metal ion concentration (Dzombak and Morel, 1990; Waite et al., 1994).

Table 5. Single mineral and component additivity SCM parameters.

Model	Surface species	Exponents in mass law defining the surface species [±]						Log K_f (I = 0)
		a	b	c	d	e	f	
Quartz TLM [⊗] 0.005–0.1M NaNO_3 U(VI): 10^{-8} – 10^{-5} M pH: 3.5–9.0 $p\text{CO}_2$: air–7.5%	SO^-	1	–1			–1		–8.340
	SONa	1	–1			–1	1	–6.51
	$\text{SO}_{\text{strong}}\text{UO}_2^+$	1	–1		1	1		2.13
	$\text{SO}_{\text{weak}}\text{UO}_2^+$	1	–1		1	1		–1.91
	$\text{SO}_{\text{strong}}\text{UO}_2\text{OH}$	1	–2		1			–1.92
	$\text{SO}_{\text{weak}}\text{UO}_2\text{OH}$	1	–2		1			–5.83
	$\text{SOUO}_2(\text{OH})(\text{CO}_3)^{2-}$	1	–4	1	1	–0.25	–1.75	–14.08
Ferrihydrite DLM [⊕] 0.004–0.5M NaNO_3 U(VI): 10^{-8} – 10^{-4} M pH: 3.5–9.0 $p\text{CO}_2$: air–1%	SOH_2^+	1	1			1		6.62
	SO^-	1	–1			–1		–9.24
	SCO_3^-	1	–1	1		–1		–5.31
	SCO_3H	1		1				2.90
	$(\text{SO}_{\text{strong}})_2\text{UO}_2$	1	–2		1			–2.45
	$(\text{SO}_{\text{weak}})_2\text{UO}_2$	1	–2		1			–6.05
	$(\text{SO}_{\text{strong}})_2\text{UO}_2\text{CO}_3^{2-}$	1	–4	1	1	–2		–12.26
Goethite TLM [∩] 0.1M NaClO_4 U(VI): 10^{-6} M pH: 3.5–9.5 $p\text{CO}_2$: 0–2%	$(\text{SO}_{\text{weak}})_2\text{UO}_2\text{CO}_3^{2-}$	1	–4	1	1	–2		–16.35
	SOH_2^+	1	1			1		6.90
	$\text{SOH}_2^+\text{Cl}^-$	1	1			1	–1	8.38
	SO^-	1	–1			–1		–10.90
	SONa	1	–1			–1	1	–9.29
	S_2CO_3^-	1	–1	1		–0.2	–0.8	–3.24
	$\text{S}_2\text{CO}_3\text{H}$	1		1				2.55
Montmorillonite DLM [⊙] 0.1M NaNO_3 U(VI): $2 \cdot 10^{-7}$ to $2 \cdot 10^{-6}$ M pH: 2–9 $p\text{CO}_2$: air	$\text{S}_2\text{CO}_3\text{Na}$	1	–1	1				–4.75
	$(\text{SO})_2\text{UO}_2$	1	–2		1			–4.71
	$(\text{SO})_2\text{UO}_2(\text{CO}_3)_2^{4-}$	1	–6	2	1	–2	–2	–22.80
	AlOH_2^+	1	1			1		8.44
	AlO^-	1	–1			–1		–9.84
	SiO^-	1	–1			–1		–7.31
	AlOUO_2^+	1	–1		1	1		3.03
Montmorillonite DLM [⊙] 0.1M NaNO_3 U(VI): $2 \cdot 10^{-7}$ to $2 \cdot 10^{-6}$ M pH: 2–9 $p\text{CO}_2$: air	SiOUO_2^+	1	–1		1	1		2.94
	$\text{AlO}(\text{UO}_2)_3(\text{OH})_5$	1	–6		3			–14.27
	$\text{SiO}(\text{UO}_2)_3(\text{OH})_5$	1	–6		3			–14.61

[±] Mass law for formation of the surface species is: $[\text{Surface species}] = K_f[\text{SOH}]^a(\text{H}^+)^b(\text{H}_2\text{CO}_3)^c(\text{UO}_2^{2+})^d \exp\{(-F/RT)(e\psi_o + f\psi_p)\}$. Coefficients for Na^+ and Cl^- not shown.

[⊗] Kohler et al., 2004b, TLM = triple layer model, $C_1 = 1.0$ Farads/m², $C_2 = 0.2$ Farads/m², total sites = 7.657 $\mu\text{moles/m}^2$; strong sites = 0.00268 $\mu\text{moles/m}^2$.

[⊕] Waite et al., 1994, DLM = diffuse layer model; total sites = 0.875 moles sites/mole Fe(III); strong sites = 0.00184 moles sites/mole Fe(III); U(VI) surface species form bidentate bonds that consume two surface sites in mass balance for sites but have an exponent of one in the mass law.

[∩] Villalobos et al., 2001, TLM, $C_1 = 1.2$ Farads/m², $C_2 = 0.2$ Farads/m², total sites = 16.62 $\mu\text{moles/m}^2$; U(VI) and carbonate surface species form bidentate bonds that consume two surface sites in mass balance for sites but have an exponent of one in the mass law.

[⊙] Pabalan et al., 1998, DLM, total sites = 3.84 $\mu\text{moles/m}^2$; ratio of aluminol to silanol sites = 0.83; edge surface area = 10% of montmorillonite surface area; ion exchange neglected.

Application of the models to predict U(VI) adsorption on the quartz in the Naturita sediments requires that the number of silanol sites per liter of water be known. As mentioned above, the Naturita sediments are 36.6 and 3.97% Si and Al by weight, respectively. If we assume that all Al is present primarily in montmorillonite, then we can roughly estimate that montmorillonite Si is $\sim 8.3\%$ of the sediment by weight (McKinley et al., 1995). We assume the remaining Si (28.3%) is present in quartz, which represents 64.6% (as SiO_2) by weight of the sediments. As a starting point for the calculations, we assume arbitrarily that quartz also represents 64.6% of the sediment surface area.

Figure 7 shows the predictions for U(VI) adsorption by the estimated quartz component of the sediments (expressed as $\log K_d$ values) for the chemical conditions present in the U(VI) batch adsorption experiments. The predicted U(VI) adsorption is very good for the experiments with the highest $p\text{CO}_2$ (6.8%), and the $\log K_d$ values are reasonable for the data equilibrated at 0.05% $p\text{CO}_2$, although the slope of the latter curve is too shallow. The agreement at the intermediate values of $p\text{CO}_2$ was not as good, with a typical error of ~ 0.3 log units between the calculated and measured K_d values. The disagreement at intermediate values of $p\text{CO}_2$ may be due to the fact the original quartz study (Kohler et al., 2004b) only included experimental data at two $p\text{CO}_2$ values (air and 7.5%). If additional data were collected in the quartz system at intermediate values of $p\text{CO}_2$, perhaps the prediction for the Naturita sediments would be improved.

Although the predicted U(VI) adsorption was reasonable assuming that the quartz surface represented most (64.6%) of the sediment BET surface area, this assumption is questionable.

Quartz grains in sediments generally have a much lower surface area than that measured for the Naturita sediments ($5.15 \text{ m}^2/\text{g}$), usually in the range of $0.1\text{--}0.4 \text{ m}^2/\text{g}$ (e.g., Coston et al., 1995). Thus, the actual surface area of quartz in the sediments is likely overestimated significantly by equating it proportionally to the percent weight abundance of quartz. In addition, because of the extensive coatings present on the surface of the quartz grains in the Naturita sediments (Fig. 4), it is likely that a significant fraction of the quartz surface area is coated with illite/smectite clay (Sanpawanitchakit, 2002; Jove-Colon et al., 2004), which may make a large proportion of the silanol groups unavailable for U(VI) adsorption reactions.

To make a qualitative prediction of U(VI) adsorption by smectite in the Naturita sediments, we assumed arbitrarily that 90% ($4.64 \text{ m}^2/\text{g}$) of the sediment BET surface area was due to montmorillonite. Assuming the montmorillonite has a specific surface area of $100 \text{ m}^2/\text{g}$ (Turner et al., 1996; Pabalan et al., 1998), this would mean that the Naturita sediment contained 46 mg of montmorillonite per g of Naturita sediment. Assuming that the montmorillonite is $\sim 21\%$ Al by weight (McKinley et al., 1995), the montmorillonite Al would be 0.97% by weight of the sediment. This represents $\sim 25\%$ of the Al in the Naturita sediments, which seems a plausible estimate.

Figure 8 shows diffuse layer model (DLM) predictions for U(VI) adsorption by montmorillonite for the chemical conditions present in the Naturita sediment experiments, using the model of Pabalan et al. (1998). Because the basal planes of the montmorillonite do not have functional groups that form complexes with U(VI) (Pabalan et al., 1998), a significant portion of the surface area measured by the BET method might not be available for adsorption of U(VI). Following the model of

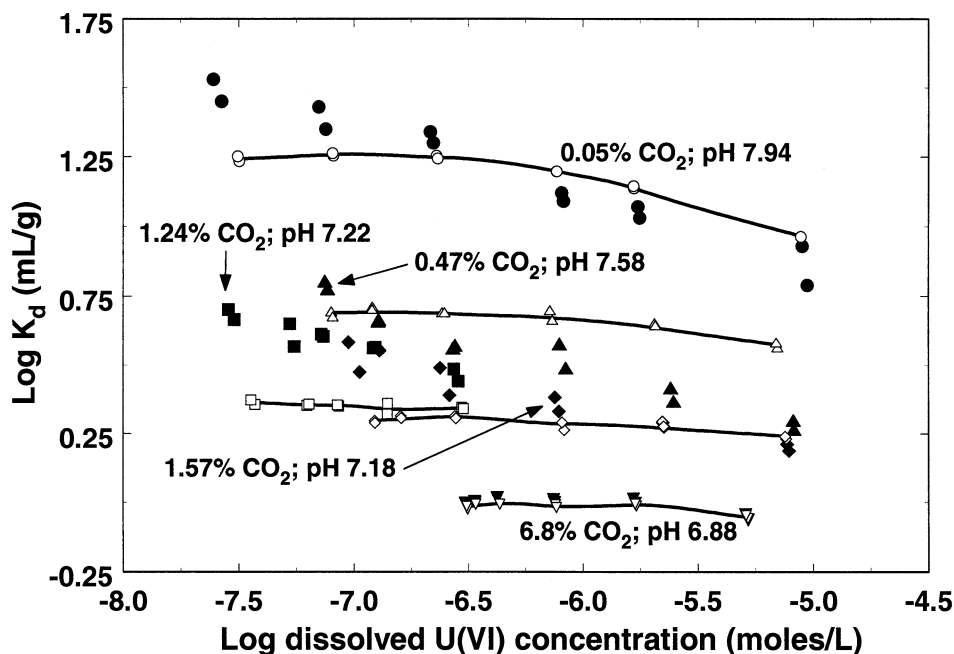


Fig. 7. Predictions of U(VI) adsorption with the quartz triple layer SCM of Kohler et al. (2004b). Experimental data for the NABS sample (shown as solid symbols) are the same as in Figure 6b. Model calculations were made at the same chemical conditions and for quartz surface areas (m^2/L) equal to 64.6% of those in the NABS experiments. The quartz model predictions are shown as smoothed solid curves drawn through the open symbols. Each symbol type is for the same set of chemical conditions (e.g., circles are for 0.05% CO_2 , pH 7.94; solid = experimental and open = model).

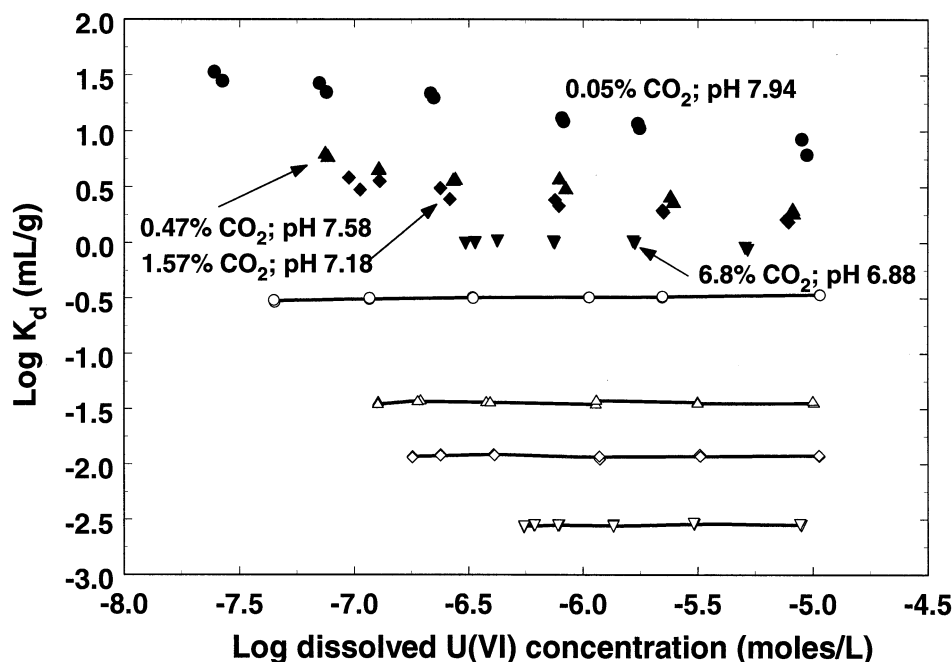


Fig. 8. Predictions of U(VI) adsorption with the montmorillonite diffuse layer SCM of Pabalan et al. (1998). Experimental data for the NABS sample (shown as solid symbols) are the same as in Figure 6b. Model predictions were made at the same chemical conditions and assuming that 90% of the sediment surface area was due to montmorillonite. The montmorillonite model predictions are shown as smoothed solid curves drawn through the open symbols. Each symbol type is for the same set of chemical conditions (e.g., upward triangles are for 0.47% CO₂, pH 7.58; solid = experimental and open = model).

Pabalan et al. (1998), only the edge site surface area was considered in the predictions (assumed to be 10% of the BET surface area), so in this case, the montmorillonite edge surface area was 0.464 m²/g of sediment. The model predictions greatly underestimate the experimental data at all pCO₂ values. This suggests that U(VI) adsorption on the illite/smectite coatings on the Naturita sediment grains is too weak to account for the overall observations of U(VI) adsorption by the sediments. By comparison, Turner et al. (1996) overpredicted U(VI) adsorption by a subsurface mineral isolate when using gibbsite as a model for surface aluminol groups.

As can be seen from the calculations above, one of the most difficult issues in applying the SCM concept to sediments and soils is determining (or estimating) the type and relative abundance of mineral functional groups on the adsorbing surfaces. In a study of Cape Cod aquifer sediments, it was found that a good estimation of the chemical composition of grain coatings could be obtained by hot (100°C) 4M HCl extraction of several hundred quartz grains, picked by hand under an optical microscope (Coston et al., 1995). Isolation of the separate quartz mineral fraction was critical in determining the composition of the coatings by this method, because the strong acid would otherwise dissolve significant quantities of Fe, Al, and other elements present in discrete grains of feldspars, goethite, hematite, magnetite, and other minerals, rather than in coating mineral phases (Davis et al., 1998).

Table 6 shows the quantities of Fe and Al dissolved in a hot 4M HCl extraction of quartz grains picked from the Naturita sediment sample and for other extractions of the complete NABS sediment sample (Sanpawanitchakit, 2002; Davis and Curtis, 2003). The 72-h hydroxylamine hydrochloride (HH)

extraction is designed to determine the quantity of crystalline iron oxides present in soils (Chao and Zhou, 1983). Note that the 72-h HH extraction of the NABS sample dissolved 13 and 23 times the amount of Fe and Al, respectively, as the much stronger hot 4M HCl extraction dissolved from the separated quartz grains. This demonstrates the usefulness of the tedious procedure of isolating quartz grains to estimate the composition of grain coatings, in that strong extractions on the whole sediment sample would yield gross overestimates of the elements present in the quartz coatings. The 0.5-h HH extraction is often used to estimate the ferrihydrite or poorly crystalline iron oxyhydroxide abundance in soils (Chao and Zhou, 1983).

Table 6. Results of chemical extractions of the NABS sediment sample.

NABS sample (<3 mm) Extraction	μmoles/g			
	Fe	Al	Si	Mn
Acetate buffer (pH 5) ^{II}	3.44	4.12	3.94	1.75
0.5 hr Hydroxylamine Hydrochloride [‡]	8.71	16.7	21.7	1.89
72 hr Hydroxylamine Hydrochloride [‡]	95	125	92.9	2.82
72 hr hot concentrated HNO ₃ [‡]	288	437	na ⁺	5.02
Hand-picked quartz grains from NABS	μmoles/g			
4M HCl at 100°C ^{II}	7.33	5.29	na	na

^{II} Data from Sanpawanitchakit (2002).

[‡] Data from Davis and Curtis (2003).

⁺ Not analyzed.

Interestingly, the 0.5-h HH extraction of the whole sample and the hot 4M HCl extraction of quartz grains yielded similar amounts of dissolved Fe. If one assumes that the Fe dissolved in the 0.5-h HH extraction is derived from ferrihydrite dissolution and that most of the ferrihydrite is present as quartz grain coatings, the results suggest that most of the Fe in the quartz grain coatings is ferrihydrite, rather than goethite or hematite. However, Jove-Colon et al. (2004) observed considerable amounts of both ferrihydrite and goethite in the Naturita grain coatings (Fig. 4).

Waite et al. (1994) developed a DLM to describe U(VI) adsorption on ferrihydrite in NaNO₃ solution as a function of pH, ionic strength, U(VI) concentration, and the partial pressure of CO₂ (Table 5). To make predictions with this model we assumed that all of the Fe in the quartz coatings (7.33 μmoles/g, Table 6) was present as ferrihydrite, and that similar coatings existed on all sediment grains. Figure 9a shows the DLM predictions for U(VI) adsorption by ferrihydrite for the chemical conditions present in the Naturita sediment experiments. The predicted U(VI) adsorption underestimated the experimental observations slightly at the two lowest pCO₂ values, but the predictions were badly underestimated (more than an order of magnitude) at the higher pCO₂ values.

A similar approach was used to predict U(VI) adsorption by the coatings, assuming that all of the Fe in the coating was present as goethite (Fig. 9b) and using the TLM of Villalobos et al. (2001). Adsorption was significantly overpredicted at the lowest pCO₂ value and underpredicted at the highest pCO₂ value. Agreement between the experimental data and model predictions was good at the intermediate pCO₂ values.

The predicted curves for the two iron oxide minerals (Figs. 9a and 9b) show a much stronger dependence on the partial pressure of carbon dioxide than observed in the experimental data or in the previous model predictions for quartz and montmorillonite. The influence of carbonate on U(VI) adsorption on iron oxides is complex, in that carbonate anions adsorb and change the electrical double layer charge and potential of iron oxides (Lumsdon and Evans, 1994; Villalobos and Leckie, 2001), and U(VI) adsorbs as ternary uranyl-carbonate-surface complexes (Bargar et al., 2000). Although the predicted K_d values for U(VI) adsorption on iron oxides in the grain coatings are of the right order of magnitude, the spread in the values as a function of pCO₂ is too large, suggesting either that there are compensating effects on the sediments surfaces or that the Waite and Villalobos models are not yet sufficiently robust to predict the effects of carbonate over such a large range in pCO₂ values.

The predictive calculations shown above were each made for a single mineral phase. In a true Component Additivity prediction, all of the mineral phases should be considered simultaneously in an equilibrium calculation. One of the issues involved in making such a model calculation is the available software. For example, in the calculations presented above, the models in the literature that were considered best for U(VI) adsorption on quartz and goethite were triple layer models, while those for ferrihydrite and montmorillonite were diffuse layer models. FITEQL (and to our knowledge, other computer programs that consider surface complexation reactions) does not allow the combination of triple layer and diffuse layer models within the same computation.

To demonstrate a true Component Additivity prediction, the software problem was addressed by calibrating a triple layer model for U(VI) adsorption on ferrihydrite using the original data of Waite et al. (1994) and the triple layer model for ferrihydrite of Davis and Leckie (1978). Figure 10 shows a CA model prediction of U(VI) adsorption on the Naturita sediment, assuming that 30% of the sediment surface area was due to quartz and that the sediment contained 20 μmoles/g of both ferrihydrite and goethite. Adsorption was overpredicted at low pCO₂ values, due to strong adsorption predicted on the goethite component. Agreement between the experimental data and model predictions was reasonable at the intermediate and high pCO₂ values. Agreement between the experimental data and model predictions in other calculations varied substantially (not shown), depending upon the assumptions made about the relative amounts of surface area of quartz, ferrihydrite, and goethite in the sediments.

3.4. Generalized Composite Model for U(VI) Adsorption on Naturita Sediments

As was shown above, predicting U(VI) adsorption on the Naturita sediments based on published SCM for single mineral phases in simple electrolyte solutions is possible if simplifying assumptions are made (Fig. 10). Whether the agreement between the model predictions and experimental data is adequate depends on the objective of the modeling exercise. For example, given the geochemical complexity of the sediments, one might consider the agreement between the simple quartz model calculations and the experimental data to be surprisingly good (Fig. 7). On the other hand, the differences between the calculated and experimental K_d values (Fig. 10) might be considered too large and unpredictable to be used in reactive transport simulations for regulatory risk assessments. The complex aqueous chemistry of U(VI) and variable chemical conditions clearly cause variable K_d values for U(VI) in the Naturita aquifer, and thus a surface complexation model (rather than a constant-K_d model) is needed to describe U(VI) transport in the aquifer (Davis and Curtis, 2003; Curtis et al., 2004). To meet this objective, a Generalized Composite (GC) SCM was developed based on a semiempirical fit to the experimental data for U(VI) adsorption by the Naturita sediments. In the GC approach, laboratory experiments are conducted with sediments from the field site to be modeled, and mass law relationships are derived that describe the change in metal ion adsorption with variations in groundwater chemical conditions observed or anticipated in the aquifer (Davis et al., 1998; Davis et al., 2002).

Because no electrostatic information was available for the charge and potential on Naturita sediment surfaces, a non-electrostatic GC model was used. In principle, potentiometric titration can be used to determine the surface proton balance of soils and sediments (Charlet and Sposito, 1987), as is commonly done to determine surface charge on pure, insoluble mineral phases, such as goethite (Lützenkirchen et al., 2002). However, the interpretation of the titration data is complex in the case of soils and sediments, because the consumption of titrant is often dominated by the dissolution of mineral phases, the release of organic acids, or other adsorption/desorption reactions. For the Naturita sediments, for example, acid-base

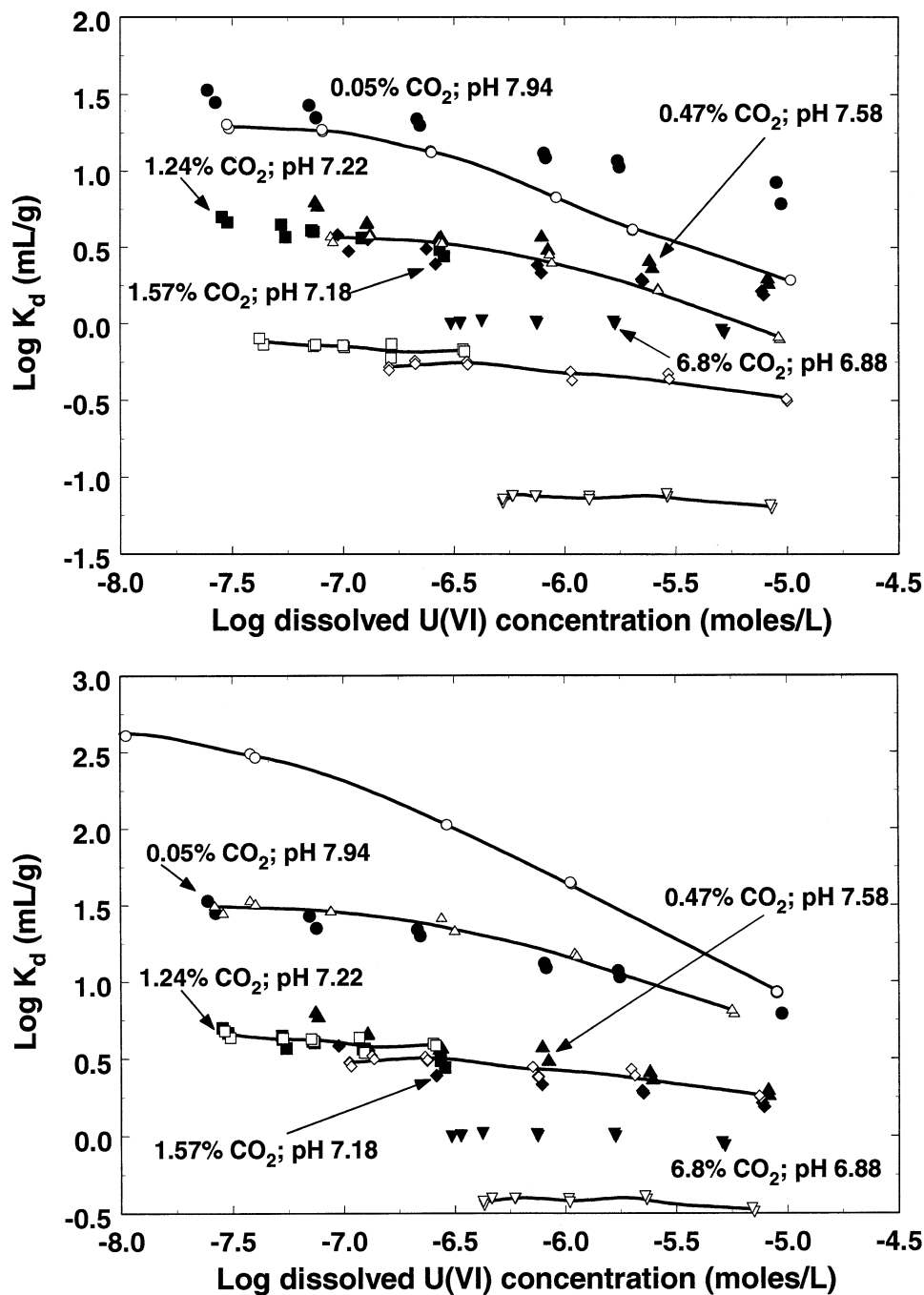


Fig. 9. a) Predictions of U(VI) adsorption with the ferrihydrite diffuse layer SCM of Waite et al. (1994). Experimental data for the NABS sample (shown as solid symbols) are the same as in Figure 6b. Model predictions were made at the same chemical conditions and assuming that all of the iron dissolved from Naturita quartz grain coatings was present as ferrihydrite. The ferrihydrite model predictions are shown as smoothed solid curves drawn through the open symbols. Each symbol type is for the same set of chemical conditions (e.g., squares are for 1.24% CO_2 , pH 7.22; solid = experimental and open = model). b) Predictions of U(VI) adsorption with the goethite TLM of Villalobos et al. (2001). Experimental data for the NABS sample (shown as solid symbols) are the same as in Figure 6b. Model predictions were made for the same chemical conditions and assuming that all of the iron dissolved from Naturita quartz grain coatings was present as goethite. The goethite model predictions are shown as smoothed solid curves drawn through the open symbols. Each symbol type is for the same set of chemical conditions (e.g., diamonds are for 1.57% CO_2 , pH 7.18; solid = experimental and open = model).

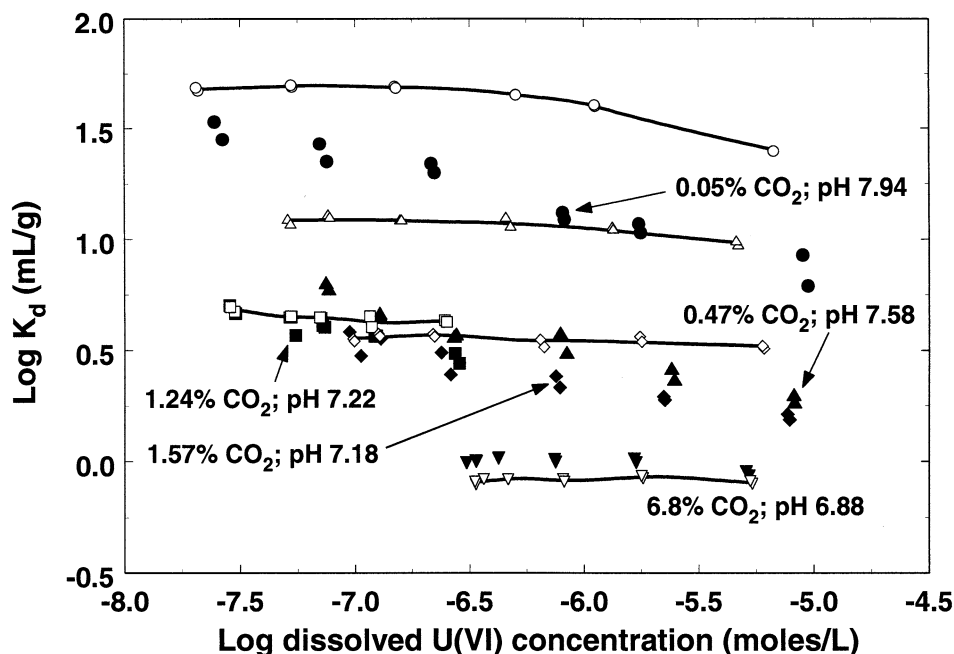


Fig. 10. Predictions of U(VI) adsorption with a Component Additivity triple layer model. Mineral components included in the calculation were quartz (assumed to comprise 30% of the sediment surface area), ferrihydrite and goethite (both assumed to be present at $20 \mu\text{moles/g}$ of sediment). Experimental data for the NABS sample (shown as solid symbols) are the same as in Figure 6b, and the model predictions were made for the same chemical conditions. The CA model predictions are shown as smoothed solid curves drawn through the open symbols. Each symbol type is for the same set of chemical conditions (e.g., downward triangles are for 6.8% CO_2 , pH 6.88; solid = experimental and open = model).

titrations would simply be dominated by calcite equilibria with the aqueous phase. Thus, the surface charge on the Naturita sediment cannot be estimated by the usual method, and the use of a non-electrostatic model simplifies the parameterization of a GC model.

To simplify the GC model further, the following decisions were made a priori: a) a total site density of $1.92 \mu\text{moles/m}^2$ was assumed (based on bidentate bonding and the recommended total site density (Davis and Kent, 1990) of $3.84 \mu\text{moles/m}^2$); b) at least two types of sites (strong and weak) were assumed to exist on the surface to account for the non-linear adsorption isotherms commonly observed for U(VI) adsorption (Waite et al., 1994), and c) it was assumed that U(VI) adsorption could be described by three or less surface reactions. The latter constraint was arbitrary but was adopted to reduce the number of model fitting parameters. In general, a goal of the semiempirical GC modeling approach is to develop the simplest model possible that describes the major features of adsorption as chemical conditions are varied over field-relevant ranges (Davis et al., 1998).

Ideally, spectroscopic data are available to constrain the possible choices of surface species. Based on the studies of Jove-Colon et al. (2004), it can be assumed that U(VI) adsorbs primarily to either aluminol edge sites and ferrinol sites located within the ubiquitous coatings found on the mineral grains. XAS and FTIR spectroscopic studies have indicated that U(VI) forms strong, edge-sharing, bidentate bonds with the surfaces of iron and aluminum oxides and edge sites of aluminosilicate minerals (Bargar et al., 2000; Moyes et al., 2000; Sylwester et al., 2000; Chisholm-Brause et al., 2001). In addition, on iron

oxide surfaces, the attached uranyl cation forms ternary surface complexes with carbonate anions (Bargar et al., 2000). Based on the spectroscopic studies, at least nine monomeric U(VI) surface reactions are possible in a uranyl/carbonate/oxide system (Table 7). Other U(VI) surface ternary complexes are plausible in the Naturita sediments, including uranyl-phosphate and -silicate ternary complexes, but these were not considered because their existence has not yet been confirmed in model systems. Because of the excess of surface sites in comparison to the U(VI) concentrations in the experiments, combined with the assumption of a non-electrostatic model, it is not necessary to consider ionization reactions of the surface hydroxyl groups (Davis et al., 1998).

Initially it was assumed that strong-binding sites were equal to 0.1% of the total sites. FITEQL calculations were completed to determine which single reaction (Table 7) would provide the best fit to the experimental data. FITEQL output includes a

Table 7. U(VI) surface reactions considered for the generalized composite SCM.

Number	Reaction
1	$\text{SOH} + \text{UO}_2^{2+} = \text{SOUO}_2^+ + \text{H}^+$
2	$\text{SOH} + \text{UO}_2^{2+} + \text{H}_2\text{O} = \text{SOUOOH} + 2\text{H}^+$
3	$\text{SOH} + \text{UO}_2^{2+} + \text{H}_2\text{CO}_3 = \text{SOUO}_2\text{HCO}_3 + 2\text{H}^+$
4	$\text{SOH} + \text{UO}_2^{2+} + \text{H}_2\text{CO}_3 = \text{SOUO}_2\text{CO}_3^- + 3\text{H}^+$
5	$\text{SOH} + \text{UO}_2^{2+} + \text{H}_2\text{CO}_3 + \text{H}_2\text{O} = \text{SOUO}_2\text{OHCO}_3^{2-} + 4\text{H}^+$
6	$\text{SOH} + \text{UO}_2^{2+} + 2\text{H}_2\text{CO}_3 = \text{SOUO}_2(\text{HCO}_3)_2^- + 3\text{H}^+$
7	$\text{SOH} + \text{UO}_2^{2+} + 2\text{H}_2\text{CO}_3 = \text{SOUO}_2(\text{CO}_3\text{HCO}_3)^{2-} + 4\text{H}^+$
8	$\text{SOH} + \text{UO}_2^{2+} + 2\text{H}_2\text{CO}_3 = \text{SOUO}_2(\text{CO}_3)_2^{3-} + 5\text{H}^+$
9	$\text{SOH} + \text{UO}_2^{2+} + 2\text{H}_2\text{CO}_3 + \text{H}_2\text{O} = \text{SOUO}_2\text{OH}(\text{CO}_3)_2^{4-} + 6\text{H}^+$

goodness-of-fit parameter, WSOS/DF, the weighted sum of squares of the difference in value between model simulations and experimental data points, divided by the degrees of freedom (Herbelin and Westall, 1999). Lower values of WSOS/DF mean the proposed model is a better fit to the data; WSOS/DF will be referred to as a “fit value” below.

Representing the U(VI) adsorption data with a single reaction produced a reasonably good fit, with the best fits (fit values = 13, 16, or 24) provided by reactions 1, 8, or 9, respectively (Table 7). The second step in model development was to consider combinations of two reactions to represent the data. In most cases, the fit to the data was improved by adding a second reaction, with the best combinations being reactions 1 and 2 (fit value = 6.1) or 8 and 9 (fit value = 12.4). Further testing showed that the results were dependent on the assumed site density for strong-binding sites. The eight best reactions pairs (fit values <22 at a strong-binding site density of 0.1% of total sites) were optimized individually to estimate the best strong-binding site density (SSD) for each pair of reactions. These results are shown in Table 8; the best fit reaction pair was reactions 1 and 2 with SSD equal to 0.06% of the total sites.

The next step in the model development was a test of whether the fit to the data was improved more by adding a third site type or a third U(VI) surface reaction. No improvement to the fit could be achieved by adding a third surface reaction to the pairs of reactions given in Table 8. However, the fit to the data was improved somewhat by adding a third site type. In the final model (shown as solid curves in Fig. 6b), reactions 1 and 2 were used with very strong sites (0.01% of the total—an assumed value) and strong sites (0.1% of the total—optimized value), resulting in a fit value of 4.5. The final GC model parameters are given in Tables 7 and 9. The reactions shown in Table 9 are written as monodentate bonds with the surface, however, the reactions can also be written as bidentate bonds as well, to be consistent with spectroscopic data (Bargar et al., 2000). This formulation changes the stability constants for the surface reactions but has a negligible effect on the goodness-of-fit to the experimental data or the choice of surface species. The reaction pairs 7 and 9 (fit value = 10.2) or 8 and 9 (fit value = 11.1) could have been chosen because these surface species are more consistent with spectroscopic data on hematite surfaces (Bargar et al., 2000). However, the reaction pair 1 and 2 was chosen as the final model because of its superior fit to the data.

The final GC model describes the batch U(VI) adsorption data quite well (Fig. 6b), but also does an excellent job of predicting K_d values for adsorbed U(VI) on uranium-contaminated Naturita sediments (Kohler et al., 2004a). In addition, it

Table 8. Best fits of surface reaction pairs and strong site density for the generalized composite SCM.

Reaction	(% of total site density)	value
1 and 2	0.06	5.0
7 and 9	0.0075	11.0
8 and 9	0.01	11.6
5 and 8	0.03	14.5
2 and 8	0.01	15.6
4 and 8	0.1	15.6
5 and 7	0.01	16.5

Table 9. Generalized composite SCM parameters.

U(VI) Surface Reaction [‡]	Log K_f (I = 0)
SSOH + UO_2^{2+} = SSOUO ₂ ⁺ + H ⁺	6.798
SOH + UO_2^{2+} = SOUO ₂ ⁺ + H ⁺	5.817
WOH + UO_2^{2+} = WOUO ₂ ⁺ + H ⁺	2.570
SSOH + UO_2^{2+} + H ₂ O = SSOUOOH + 2H ⁺	-0.671
SOH + UO_2^{2+} + H ₂ O = SOUOOH + 2H ⁺	-2.082
WOH + UO_2^{2+} + H ₂ O = WOUOOH + 2H ⁺	-5.318

[‡] Total site concentration of 1.92 μ moles/m², with SSOH denoting very strong U(VI) binding sites, SOH denoting strong binding sites, and WOH denoting weak binding sites; very strong site density of 0.01% of total sites and strong site density of 0.1% of total sites.

is very useful for predicting the transport of U(VI) in the Naturita alluvial aquifer, which has variable chemical conditions (Davis and Curtis, 2003; Curtis et al., 2004).

4. DISCUSSION

In current practice, nearly all reactive transport models ignore the geochemical complexity of contaminant plumes in groundwater systems and utilize the constant- K_d modeling approach to describe the adsorption and retardation of metal and radionuclide contaminants (USEPA, 1999; Bethke and Brady, 2000). The origin of K_d as an empirical modeling parameter can be traced to descriptions of ion exchange and ion chromatography in chemical engineering practice, primarily applied to alkali and alkaline earth cations that have extremely simple aqueous chemistry. Later, groundwater solute transport modelers assumed that this simple chemical treatment could be extended to essentially all inorganic contaminants. For example, Higgins (1959) stated that radionuclides created in underground nuclear explosions adsorbed only via an ion exchange mechanism, with “variable pH between pH 2 and 9 having a very small effect on K_d values.” K_d values may work well for elements that have simple aqueous speciation, such as Cs⁺ and Sr²⁺, and are bound primarily by ion exchange reactions, but the binding of most metals and radionuclides to mineral surfaces occurs by chemical coordination reactions with surface functional groups, such as surface hydroxyls (Davis and Kent, 1990). Baetslé (1967) argued that an exact knowledge of radionuclide adsorption isotherms was needed for accurate modeling of subsurface transport, but in the interest of computational efficiency, a constant- K_d modeling approach could be applied. Similar arguments are still made today, partly because of the perceived lack of an alternative simple modeling approach to describe adsorption and retardation as a function of variable chemical conditions in groundwater. Unfortunately, the constant- K_d approach ignores the well-developed knowledge of aqueous thermodynamics (e.g., for U(VI), Grenthe et al., 1992; Silva et al., 1995) that can be employed in geochemical models.

At field sites where there is significant temporal or spatial variation in chemical conditions, the uncertainty in simulated retardation can be reduced with the use of the semiempirical GC modeling approach (Kent et al., 2000; Davis and Curtis, 2003; Glynn, 2003).

4.1. GC Model Simulations of K_d Variation with Chemical Conditions

The GC modeling approach requires that significant chemical variations in groundwater systems are identified and that metal ion adsorption as a function of these variables is studied in the laboratory to calibrate a GC model. In this respect, the data requirements of the GC modeling approach are greater than the constant- K_d approach. To apply the GC modeling approach in reactive transport modeling, a greater emphasis must be placed on site-specific characterization of natural mineral assemblages and groundwater compositions expected to be encountered along major flowpaths away from contamination sources. A disadvantage of the GC approach (relative to CA) is that the model parameters, like K_d values, are site-specific, i.e., the values cannot be applied at other field sites.

The GC modeling approach has generally been applied using a non-electrostatic model (NEM), which considers surface equilibria strictly as chemical reactions without explicit correction for electrostatic attraction or repulsion (Davis et al., 1998; van Benschoten et al., 1998; Westall et al., 1998; Kent et al., 2000; Davis et al., 2002). In an NEM, the apparent binding constants and stoichiometry of the mass action equations are derived by fitting the *macroscopic* dependence of adsorption as a function of pH. Because of the exclusion of the electrical double layer terms, these mass action equations are not expected to provide accurate representations of the stoichiometry of the reactions *at the molecular scale*, however, the surface

reactions can still be coupled with aqueous complexation reactions to provide simulations of macroscopic adsorption as a function of aqueous chemical conditions. Even though the GC approach is semiempirical, the mass laws that account for adsorption are coupled to aqueous speciation, which is fundamentally superior to the completely empirical K_d -spline approach recommended by others (e.g., USEPA, 1999).

Based on experimental adsorption data, Davis et al. (2002) and Pabalan et al. (1998) argued that U(VI) surface complexes on oxide mineral phases and the edge sites of clays are relatively insensitive to the metal cation or surface charge of the mineral phase. These authors showed that when several mineral phases were compared on a normalized surface area basis, U(VI) adsorption varied only with aqueous speciation. Figure 11 shows calculated U(VI) K_a values (K_d divided by surface area) as a function of pH in systems equilibrated with air for: 1) selected mineral phases (quartz, ferrihydrite, hematite, and imogolite); 2) the Koongarra, Australia weathered schist (Davis et al., 2002), 3) the K_a' function of Pabalan et al. (1998), derived from the average of values for quartz, montmorillonite, and clinoptilolite; and 4) the Naturita sediment sample, at the pH value at which it equilibrated with the pCO_2 in air. The Naturita sediment U(VI) K_a value is significantly less than that observed for the other materials (Fig. 11). The result suggests that a substantial portion of the BET surface area of the Naturita sediment is not reactive with U(VI), such as the basal planes of smectites (Pabalan et al., 1998), which is consistent

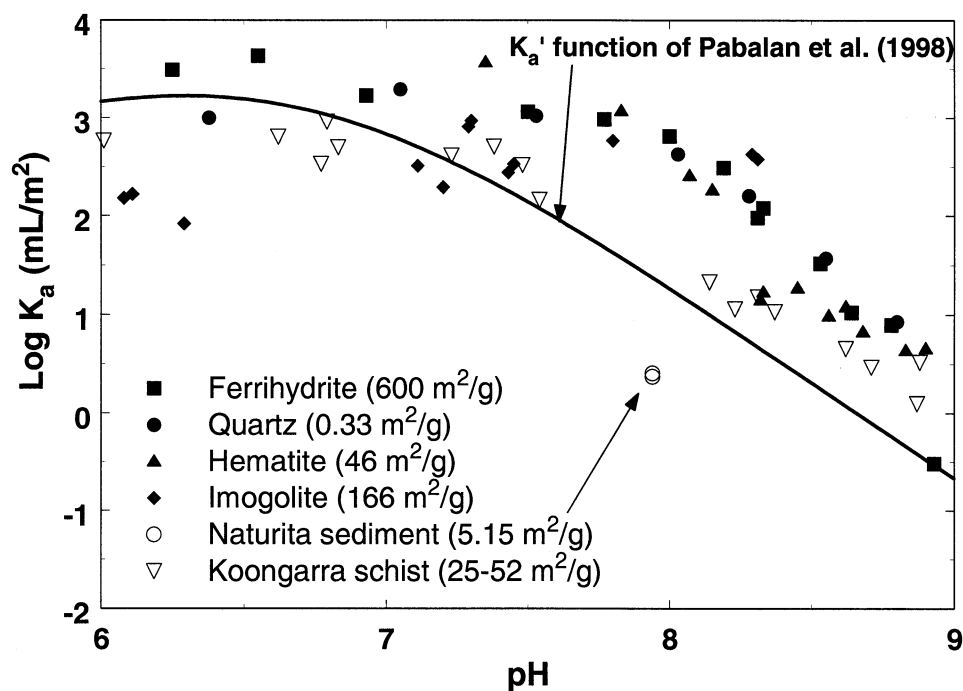


Fig. 11. Comparison of U(VI) experimental K_a (ml m^{-2}) values as a function of pH for ferrihydrite, quartz, hematite, imogolite, and Koongarra weathered schist samples in systems equilibrated with $1 \cdot 10^{-6}\text{M}$ U(VI) and atmospheric pCO_2 . Pabalan et al. (1998) calculated U(VI) K_a values for quartz, montmorillonite, and clinoptilolite for similar chemical conditions and determined a regression curve to describe the average K_a values for the three mineral phases, shown above as the K_a' function. Note that the single K_a value determined for the Naturita sediment is considerably lower in value (at the same pH value) than observed for the other mineral phases. Ferrihydrite data from Waite et al. (1994), quartz and imogolite data from Davis (2001), hematite data from Reitmeyer et al. (1999), and Koongarra schist data from Payne (1999).

with the extensive illite/smectite coatings observed by Jove-Colon et al. (2004) on the sediment grains (Fig. 4). In the K_a' function of Pabalan et al. (1998), the BET surface area of montmorillonite was multiplied by 0.1 to account for the fact that only $\sim 10\%$ of the surface area is present on the edges of clay layers. If one assumes that the surface area of the Naturita sample ($5.15 \text{ m}^2/\text{g}$) is almost entirely due to montmorillonite, then the clay edge site area would be estimated as $0.515 \text{ m}^2/\text{g}$, to be consistent with the K_a' calculation method of Pabalan et al. (1998). This would increase the K_a' value of the Naturita experimental point shown in Figure 11 by an order of magnitude, bringing it into good agreement with the K_a' function of Pabalan et al. (1998).

4.2. CA Model Simulations of K_a' Variation with Chemical Conditions

Advantages of the CA modeling approach are that the model parameters are transferable from one field site to another and that the models are supported by detailed experimental investigations published in the literature. This approach allows for the development of databases of self-consistent model parameters, tabulated for individual mineral phases (e.g., Dzombak and Morel, 1990; Sverjensky, 2001; Criscenti and Sverjensky, 2002; Sverjensky, 2003).

Unfortunately, at present, CA model predictions for soils and sediments suffer from four significant problems that likely contribute to modeling error: 1) estimation of surface site types and surface area abundances; 2) a lack of fundamental data on the effects of competitive adsorption of common groundwater solutes; 3) a lack of fundamental data on the effects of common groundwater solutes on surface charge and potentials; and 4) model consistency and software issues. Each of these problems is discussed below.

As was illustrated in the single mineral CA model predictions presented here, it is difficult to estimate the relative abundance of the surface areas of reference mineral phases that equilibrate with the solution phase. In the literature, as was done in this paper, most authors who have applied the CA approach make significant assumptions about the relative surface areas of the adsorbing phases. For example, Arnold et al. (2001) assumed that a weathered rock phyllite sample was composed of minerals (quartz, chlorite, muscovite, albite, and ferrihydrite) with relative surface areas calculated from the weight abundances of each mineral in the rock and specific surface areas (i.e., m^2/g) of the specimen minerals used in separate U(VI) adsorption studies. To make it clear to the reader, there are two major assumptions in this approach: 1) an assumption that the relative surface areas can be estimated from bulk weight abundances; and 2) an assumption that the surface area of minerals in the weathered rock, say ferrihydrite particles, is the same as the ferrihydrite used in separate laboratory investigations. Cowan et al. (1992) used a similar approach to estimate Cd(II) adsorption by the mineralogical components of an ultisol (kaolinite, 2:1 layer silicates, Al-substituted goethite, and gibbsite). Davis et al. (1998) used hot 4M HCl extractions of quartz grain coatings to determine relative abundances of Fe and Al in coatings, and used specific surface areas of synthetic ferrihydrite and amorphous alumina to estimate the adsorbent surface areas of an aquifer sand. Clearly, new experimental

methods are needed to better characterize the relative abundances of surface areas of various minerals in soils and sediments to improve CA model predictions.

The second problem stems from the fact that the models for metal ion adsorption on reference minerals are usually based on experimental datasets collected in simple electrolyte solutions. Typically, constants for the adsorption of major ions in natural waters (e.g., Mg^{2+} , Ca^{2+} , CO_3^{2-} , SO_4^{2-} , H_4SiO_4) are not available for the reference minerals, and thus, these reactions are usually ignored in CA model calculations for actual groundwaters. This could cause errors in CA model calculations due to at least two complex factors: 1) adsorption could be overestimated by ignoring competitive adsorption reactions of the major ions; or 2) adsorption could be underestimated because a ternary surface species forms that was not previously known (e.g., Bargar et al., 2000). Improvement of CA model predictions could be made if datasets for metal ion adsorption on reference minerals were available in solutions with composition typical of natural waters.

The third problem is related to the second, in that SCM parameters for metal ion adsorption on reference minerals are usually based on mass action equations that correct for coulombic effects only in simple electrolyte solutions. It is known that the surface charge of mineral phases in natural waters can be quite different from that observed in simple electrolyte solutions. The adsorption of major ions and organic acids in natural waters is known to cause large changes in the point-of-zero-charge (pH_{PZC}) and isoelectric point (pH_{IEP}) of mineral phases (Fuerstenau et al., 1981; Davis, 1982; Davis and Kent, 1990). In the CA calculations illustrated in this paper and elsewhere in the literature, it is assumed that the surface charge and potential of a mineral in the sediment, say ferrihydrite, can be predicted from what was observed for ferrihydrite in simple 1:1 electrolyte solutions. This means that adsorption reactions of Ca^{2+} , Mg^{2+} , and other ions in the water (including fulvic acids) do not significantly affect the surface potential of ferrihydrite as a function of pH in the CA model predictions. Another problem in the modeling of the EDL properties is that the effects of overlapping double layers in secondary mineral coatings are poorly understood. For example, if goethite nanoparticles are present as an overgrowth on a quartz surface, is the goethite EDL significantly affected by the underlying quartz surface? It is clear that assumptions about EDL properties must cause an error in CA model calculations, but the magnitude of this error is unknown. More experimental data are needed for the EDL properties of reference minerals suspended in solutions of composition typical of natural waters, so that the extrapolation from laboratory data to natural systems is less uncertain.

The fourth problem involves model consistency and available software. Presently programs such as FITEQL require that all of the models for component minerals use the same electrical double layer model (e.g., diffuse layer or triple layer models). Moreover, when using the triple layer model, each component mineral model must have the same inner layer capacitance value, and it is not possible to consider electrical potentials individually for each mineral phase within the same computation. Thus, in the CA model calculation illustrated in Figure 10, the surface and beta layer potentials were calculated for the mixture as a whole, and each mineral component then

had the same equilibrium surface and beta layer potentials for a given set of chemical conditions. Clearly it is unlikely that the electrical double layers of individual minerals overlap and interact to this extent; software is needed that will allow the surface potentials for each mineral phase to be calculated separately in a single equilibrium calculation.

In the opinion of the authors, the problems listed above were responsible for most of the uncertainty in U(VI) adsorption predicted in the CA model calculations (Figs. 7–10) in comparison to the experimental data.

5. CONCLUDING REMARKS

Adsorption of U(VI) by the Naturita aquifer sediments was strongly influenced by the $p\text{CO}_2$ in equilibrium with the aqueous phase. Under conditions typical of groundwater at the field site in Naturita ($p\text{CO}_2$ of 2–6%, pH 7), the K_d value for U(VI) adsorption was on the order of ten times less than that observed when systems were equilibrated with air. This illustrates the importance of $p\text{CO}_2$ in experiments designed to determine K_d values; most K_d values for U(VI) in the literature have been determined in systems exposed to air (USEPA, 1999).

Although our understanding of the bonding of adsorbed species is well advanced at the molecular level in clean mineral suspensions (e.g., Bargar et al., 2000), our knowledge is increasingly uncertain as the physical scale and complexity increase. The complex physical chemistry at the mineral-water interface in natural systems makes it difficult to apply the detailed molecular scale knowledge of surface speciation on single mineral phases directly to simulations of adsorption in the groundwater environment. Because micron-thick coatings of secondary mineral phases and resistant organic materials commonly occur on sediment surfaces, our knowledge of the chemical composition of the surface region is poor. Even if it can be demonstrated that adsorption is dominated by, for example, nano-sized iron oxide particles in such coatings, the surface area and electrical field on these particle surfaces is generally unknown and values must be assumed for model applications. This lack of knowledge adds considerable uncertainty to predictions of metal and radionuclide adsorption on soils and sediments using SCM from the literature that describe adsorption on clean reference mineral phases in simple electrolyte solutions.

The GC modeling approach is less chemically rigorous but allows simple relationships to be derived that couple metal and radionuclide adsorption with their aqueous speciation. Because the GC approach need not employ coulombic correction factors or surface acidity constants, it is computationally easier to incorporate the adsorption model within reactive solute transport models. Using this approach, the major features of metal and radionuclide adsorption can be simulated with a model calibrated from laboratory experiments that vary chemical conditions over field-relevant ranges (Davis and Curtis, 2003). This allows transport simulations to be conducted with less uncertainty than the constant- K_d approach, by reducing the uncertainty associated with the retardation of metals and radionuclides by adsorption. Because of the simplicity of the GC modeling approach, it may be more appropriate for reactive transport modeling at the field scale at the present time than using CA model predictions.

Acknowledgments—The authors thank Jennifer Coston, Jennifer Joye, Dave Naftz, and Walt Holmes for significant technical support during this study. The authors thank Doug Kent, Yuji Arai, and three anonymous reviewers for helpful suggestions to drafts of the manuscript. Funding for this project was provided by the U.S. Nuclear Regulatory Commission (W6813) and the U. S. Geological Survey Toxic Substances Hydrology program.

Associate editor: J. Rustad

REFERENCES

- Abdelouas A., Lutze W., and Nuttall H. E. (1999) Uranium contamination in the subsurface: Characterization and remediation. In *Uranium: Mineralogy, Geochemistry and the Environment, Reviews in Mineralogy Series, Mineralogical Society of America* Vol. 38, p. 433–473.
- Alcacio T. E., Hesterberg D., Chou J. W., Martin J. D., Beauchemin S., and Sayers D. E. (2001) Molecular scale characteristics of Cu(II) bonding in goethite-humate complexes. *Geochim. Cosmochim. Acta* 65, 1355–1366.
- Arnold T., Zorn T., Zanker H., Bernhard G., and Nitsche H. (2001) Sorption Behavior of U(VI) on Phyllite: Experiments and Modeling. *J. Contam. Hydrol.* 47, 219–231.
- Baestlé L. (1967) Computational Methods for the Prediction of Underground Movement of Radionuclides. *Nucl. Safety* 8, 576–588.
- Bargar J. R., Reitmeyer R., Lenhart J. J., and Davis J. A. (2000) Characterization of U(VI)-carbonate ternary complexes on hematite: EXAFS and electrophoretic mobility measurements. *Geochim. Cosmochim. Acta* 64, 2737–2749.
- Barnett M. O., Jardine P. M., and Brooks S. C. (2002) U(VI) Adsorption to Heterogeneous Subsurface Media. Application of a Surface Complexation Model. *Env. Sci. Technol.* 36, 937–942.
- Becker U., Rosso K. M., and Hochella M. F. (2001) The proximity effect on semiconducting mineral surfaces: A new aspect of mineral surface reactivity and surface complexation theory? *Geochim. Cosmochim. Acta* 65, 2641–2649.
- Bernhard G., Geipel G., Reich T., Brendler V., Amayri S., and Nitsche H. (2001) Uranyl(VI) carbonate complex formation. Validation of the $\text{Ca}_2\text{UO}_2(\text{CO}_3)_3$ (aq) species. *Radiochim. Acta* 89, 511–518.
- Bethke C. M. and Brady P. V. (2000) How the K_d Approach Undermines Ground Water Cleanup. *Ground Water* 38, 435–443.
- Brooks S. C., Fredrickson J. K., Carroll S. L., Kennedy D. W., Zachara J. M., Plymale A. E., Kelly S. D., Kemner K. M., and Fendorf S. (2003) Inhibition of bacterial U(VI) reduction by calcium. *Env. Sci. Technol.* 37, 1850–1858.
- Brown G. E. and Parks G. A. (2001) Sorption of Trace Elements on Mineral Surfaces: Modern Perspectives from Spectroscopic Studies and Comments on Sorption in the Marine Environment. *Intnl. Geol. Rev.* 43, 963–1073.
- Chao T. T. and Zhou L. (1983) Extraction Techniques for Selective Dissolution of Amorphous Iron Oxides from Soils and Sediments. *Soil Sci. Soc. Am. J.* 47, 225–232.
- Charlet L. and Sposito G. (1987) Monovalent ion adsorption by an oxisol. *Soil Sci. Soc. Am. J.* 51, 1155–1160.
- Chisholm-Brause C. J., Berg J. M., Matzner R. A., and Morris D. E. (2001) Uranium(VI) sorption complexes on montmorillonite as a function of solution chemistry. *J. Coll. Inter. Sci.* 233, 38–49.
- Coston J. A., Fuller C. C., and Davis J. A. (1995) Pb^{2+} and Zn^{2+} adsorption by a natural Al- and Fe-bearing surface coating on an aquifer sand. *Geochim. Cosmochim. Acta* 59, 3535–3548.
- Cowan C. E., Zachara J. M., Smith S. C., and Resch C. T. (1992) Individual sorbent contributions to cadmium sorption on ultisols of mixed mineralogy. *Soil Sci. Soc. Am. J.* 56, 1084–1094.
- Criscenti L. J. and Sverjensky D. A. (2002) A single-site model for divalent and heavy metal ion adsorption over a range of metal concentrations. *J. Coll. Inter. Sci.* 253, 329–352.
- Crowley K. D. and Ahearn J. F. (2002) Managing the Environmental Legacy of U.S. Nuclear Weapons Production. *Am. Sci.* 90, 514–523.
- Curtis G. P., Davis J. A. and Naftz D. L. (2004) Simulation of reactive transport of uranium(VI) in groundwater with variable chemical conditions. *Water Res. Res.* submitted.

- Davis J. A. (1982) Adsorption of natural dissolved organic matter at the oxide/water interface. *Geochim. Cosmochim. Acta* **46**, 2381–2393.
- Davis J. A. (2001) Surface Complexation Modeling of Uranium(VI) Adsorption on Natural Mineral Assemblages. Report NUREG/CR-6708. U. S. Nuclear Regulatory Commission, Rockville, MD.
- Davis J. A., Coston J. A., Kent D. B., and Fuller C. C. (1998) Application of the surface complexation concept to complex mineral assemblages. *Env. Sci. Tech.* **32**, 2820–2828.
- Davis J. A. and Curtis G. P. (2003) Application of Surface Complexation Modeling to Describe Uranium(VI) Adsorption and Retardation at the Uranium Mill Tailings Site at Naturita, Colorado. Report NUREG CR-6820, U. S. Nuclear Regulatory Commission, Rockville, MD. 223 pp. (Also available at <http://www.nrc.gov/reading-rm/doc-collections/nuregs/contract/cr6820/cr6820.pdf>).
- Davis J. A. and Kent D. B. (1990) Surface Complexation Modeling in Aqueous Geochemistry, Mineral-Water Interface Geochemistry. *Reviews in Mineralogy Series*, Vol. **23**, p. 177–260. Mineralogical Society of America.
- Davis J. A. and Leckie J. O. (1978) Surface ionization and complexation at the oxide/water interface. II. Surface properties of amorphous iron oxyhydroxide and adsorption of metal ions. *J. Coll. Inter. Sci.* **67**, 90–107.
- Davis J. A., Payne T. E. and Waite T. D. (2002) Simulating the pH and pCO₂ Dependence of Uranium(VI) Adsorption by a Weathered Schist with Surface Complexation Models. In *Geochemistry of Soil Radionuclides*, Special Pub. 59, pp. 61–86. Soil Science Society America, Madison, WI.
- Dzombak D. A. and Morel F. M. (1990) Surface Complexation Modeling: Hydrous Ferric Oxide. John Wiley & Sons, New York, NY.
- Fuerstenau D. W., Manmohan D., and Raghavan S. (1981) The adsorption of alkaline-earth metal ions at the rutile/aqueous interface. In *Adsorption from Aqueous Solutions* (ed. P. H. Tewari) p. 93–117. Plenum Press, New York.
- Glynn P. D. (2003) Modeling Np and Pu transport with a surface complexation model and spatially variant sorption capacities: implications for reactive transport modeling and performance assessments of nuclear waste disposal sites. *Comp. Geosci.* **29**, 331–349.
- Grenthe I., Fuger J., Konings R. J. M., Lemire R. J., Muller A. J., Nguyen-Trung C., and Wanner H. (1992) Chemical Thermodynamics of Uranium. Elsevier, Amsterdam.
- Hem J. D. (1985) Study and Interpretation of the Chemical Characteristics of Natural Water, Water-Supply Paper 2254. U.S. Geological Survey, Reston, VA, USA.
- Herbelin A. L. and Westall J. C. (1999) FITEQL: A Computer Program for the Determination of Chemical Equilibrium Constants from Experimental Data. Version 4.0, Report 99–01, Chemistry Department, Oregon State University, Corvallis, Oregon.
- Higgins G. (1959) Evaluation of the Groundwater Contamination Hazard from Underground Nuclear Explosions. *J. Geophys. Res.* **64**, 1509–1519.
- Honeyman B. D. (1984) Cation and anion adsorption at the oxide/solution interface in systems containing binary mixtures of adsorbents: An investigation of the concept of adsorptive additivity. Ph.D. Thesis, Stanford University, Stanford, CA.
- Jove-Colon C. F., Sanpawanitchakit C., Xu H., Cygan R. T., Davis J. A., Meece D. M. and Hervig R. L. (2004) A Combined Analytical Study to Characterize Uranium Soil Contamination: The Case of the Naturita UMTRA Site and the Role of Grain Coatings. NUREG Rept., U. S. Nuclear Regulatory Commission, Rockville, MD, in press.
- Kalmykov S. N. and Choppin G. R. (2000) Mixed Ca²⁺/UO₂²⁺/CO₃²⁻ complex formation at different ionic strengths. *Radiochim. Acta* **88**, 603–606.
- Kent D. B., Abrams R. H., Davis J. A., Coston J. A., and LeBlanc D. R. (2000) Modeling the influence of variable pH on the transport of zinc in a contaminated aquifer using semi-empirical surface complexation models. *Water Res. Res.* **36**, 3411–3425.
- Kohler M., Curtis G. P., Kent D. B., and Davis J. A. (1996) Experimental investigation and modeling of uranium(VI) transport under variable chemical conditions. *Water Res. Res.* **32**, 3539–3551.
- Kohler M., Honeyman B. D., and Leckie J. O. (1999) Neptunium(V) Sorption on Hematite (α -Fe₂O₃) in Aqueous Suspension: The effect of CO₂. *Radiochim. Acta* **85**, 33–48.
- Kohler M., Meece D. M., Curtis G. P., and Davis J. A. (2004a) Methods for estimating adsorbed uranium(VI) and distribution coefficients in contaminated sediments. *Env. Sci. Tech.* **38**, 240–247.
- Kohler M., Davis J. A. and Curtis G. P. (2004b) Modeling adsorption of U(VI) on quartz at variable pH, carbonate and fluoride concentrations. *J. Coll. Inter. Sci.* in preparation.
- Koretsky C. (2000) The significance of surface complexation reactions in hydrologic systems: A geochemist's perspective. *J. Hydrol.* **230**, 127–171.
- Lenhart J. J., Cabaniss S. E., MacCarthy P., and Honeyman B. D. (2000) Uranium(VI) complexation with citric, humic and fulvic acids. *Radiochim. Acta* **88**, 345–353.
- Lumsdon D. G. and Evans L. J. (1994) Surface complexation model parameters for goethite (α -FeOOH). *J. Coll. Inter. Sci.* **164**, 119–125.
- Lützenkirchen J., Boily J.-F., Lövgren L., and Sjöberg S. (2002) Limitations of the potentiometric titration technique in determining the proton active site density of goethite surfaces. *Geochim. Cosmochim. Acta* **66**, 3389–3396.
- McKinley J. P., Zachara J. M., Smith S. C., and Turner G. D. (1995) The influence of uranyl hydrolysis and multiple site-binding reactions on adsorption of U(VI) to montmorillonite. *Clays Clay Min.* **43**, 586–598.
- Moll H. (1997) Zur Wechselwirkung von Uran mit Silicat in Wässrigen Systemen, Ph.D. Thesis, Technische Universität Dresden, Germany.
- Moyes L. N., Parkman R. H., Charnock J. M., Vaughan D. J., Livens F. R., Hughes C. R., and Braithwaite A. (2000) Uranium uptake from aqueous solution by interaction with goethite, lepidocrocite, muscovite, and mackinawite: An X-ray absorption spectroscopy study. *Env. Sci. Tech.* **34**, 1062–1068.
- Pabalan R. T., Turner D. R., Bertetti F. P. and Prikryl J. D. (1998) Uranium(VI) Sorption onto Selected Mineral Surfaces: Key Geochemical Parameters. In *Adsorption of Metals by Geomedia* Academic Press, p. 99–130.
- Padmanabhan E. and Mermut A. R. (1996) Submicroscopic Structure of Fe-coatings on Quartz Grains in Tropical Environments. *Clays Clay Min.* **44**, 801–810.
- Papelis C, Hayes K. F. and Leckie J. O. (1988) HYDRAQL: A program for the computation of chemical equilibrium composition of aqueous batch systems including surface complexation modeling of ion adsorption at the oxide/solution interface. *Tech. Rept.* **306**, Dept. of Civil Engineering, Stanford University, Stanford, California, USA.
- Papini M. P., Kahie Y. D., Troia B., and Majone M. (1999) Adsorption of Lead at Variable pH onto a Natural Porous Medium: Modeling of Batch and Column Experiments. *Env. Sci. Tech.* **33**, 4457–4464.
- Parkhurst D. L., Stollenwerk K. G. and Colman J. A. (2003) Reactive-transport of phosphorus in the sewage plume at the Massachusetts Military Reservation, Cape Cod, Massachusetts. *Water-Resources Investigations Report* 03-4017, U. S. Geological Survey.
- Payne T. E. (1999) Uranium (VI) interactions with mineral surfaces: Controlling factors and surface complexation modeling. Ph.D. Thesis. University of New South Wales, Australia.
- Penn R. L., Zhu C., and Veblen D. R. (2001) Iron Oxide Coatings on Sand Grains from the Atlantic Coastal Plain: High-resolution Transmission Electron Microscopy Characterization. *Geology* **29**, 843–846.
- Prikryl J. D., Jain A., Turner D. R., and Pabalan R. T. (2001) Uranium(VI) Sorption Behavior on Silicate Mineral Mixtures. *J. Contam. Hydrol.* **47**, 241–253.
- Read D., Ross D., and Sims R. J. (1998) The Migration of uranium through Clashach Sandstone: the role of low molecular weight organics in enhancing radionuclide transport. *J. Contam. Hydrol.* **35**, 235–248.
- Reitmeyer R., Davis J. A., and Bargar J. R. (1999) A spectroscopic approach to surface complexation modeling of uranyl carbonates on Fe-oxide surfaces. Proceedings, American Chemical Society 217th National Meeting. Anaheim, CA.
- Riley R. G., Zachara J. M and Wobber F. J. (1992) Chemical Contaminants on DOE Lands and Selection of Contaminant Mixtures for Subsurface Science Research. Report DOE/ER-0547T, U. S. Department of Energy.
- Sandino A. and Bruno J. (1992) The Solubility of (UO₂)₃(PO₄)₂·4H₂O_(s) and the Formation of U(VI) Phosphate Complexes: Their

- Influence in Uranium Speciation in Natural Waters. *Geochim. Cosmochim. Acta* **56**, 4135–4145.
- Sanpawanitchakit C. (2002) The application of surface complexation modeling to the adsorption of uranium (VI) on natural composite materials. PhD Thesis, Colorado School of Mines, Environmental Science and Engineering, Golden, Co., USA.
- Schmeide K., Pompe S., Bubner M., Heise K. H., Bernhard G., and Nitsche H. (2000) Uranium(VI) sorption onto phyllite and selected minerals in the presence of humic acid. *Radiochim. Acta* **88**, 723–728.
- Silva R. J. (1992) Mechanisms for the Retardation of Uranium(VI) Migration. *Mat. Res. Soc. Symp. Proc.* **Vol. 257**, 323–330.
- Silva R. J., Bidoglio G., Rand M. H., Robouch P. B., Wanner H., and Puigdomenech I. (1995) Chemical Thermodynamics of Americium, with an appendix on Chemical Thermodynamics of Uranium. Nuclear Energy Agency, OECD. Elsevier, North-Holland.
- Stollenwerk K. G. (1998) Molybdate Transport in a Chemically Complex Aquifer; Field Measurements Compared with Solute-transport Model Predictions. *Water Res. Res.* **34**, 2727–2740.
- Sverjensky D. A. (2001) Interpretation and prediction of triple-layer model capacitances and the structure of the oxide-electrolyte-water interface. *Geochim. Cosmochim. Acta* **65**, 3643–3655.
- Sverjensky D. A. (2003) Standard states for the activities of mineral surface-sites and species. *Geochim. Cosmochim. Acta* **67**, 17–28.
- Sylwester E. R., Hudson E. A., and Allen P. G. (2000) The structure of uranium (VI) sorption complexes on silica, alumina, and montmorillonite. *Geochim. Cosmochim. Acta* **64**, 2431–2438.
- Turner G. D., Zachara J. M., McKinley J. P., and Smith S. C. (1996) Surface-charge Properties and UO_2^{2+} Adsorption of a Subsurface Smectite. *Geochim. Cosmochim. Acta* **60**, 3399–3414.
- USDOE(1996) Programmatic Environmental Impact Statement for the Uranium Mill Tailings Remedial Action Ground Water Project. Report DOE/EIS-0198, Vol. I, U.S. Department of Energy, Grand Junction Office.
- USEPA(1999) Understanding Variation in Partition Coefficient, K_d , Values. Vol. 1, Report EPA 402-R-99–0044A, Washington, DC.
- van Benschoten J. E., Young W. H., Matsumoto M. R., and Reed B. E. (1998) A nonelectrostatic surface complexation model for lead sorption on soils and mineral surfaces. *J. Environ. Qual.* **27**, 24–30.
- Villalobos M. and Leckie J. O. (2001) Surface complexation modeling and FTIR study of carbonate adsorption on goethite. *J. Coll. Inter. Sci.* **235**, 15–32.
- Villalobos M., Trotz M. A., and Leckie J. O. (2001) Surface complexation modeling of carbonate effects on the adsorption of Cr(VI), Pb(II), and U(VI) on goethite. *Env. Sci. Tech.* **35**, 3849–3856.
- Waite T. D., Davis J. A., Payne T. E., Waychunas G. A., and Xu N. (1994) Uranium(VI) adsorption to ferrihydrite: Application of a surface complexation model. *Geochim. Cosmochim. Acta* **58**, 5465–5478.
- Waite T. D., Davis J. A., Fenton B. R., and Payne T. E. (2000) Approaches to Modelling Uranium(VI) Adsorption on Natural Mineral Assemblages. *Radiochim. Acta* **88**, 687–699.
- Wazne M., Korfiatis G. P., and Meng X. (2003) Carbonate effects on hexavalent uranium adsorption by iron oxyhydroxide. *Env. Sci. Tech.* **37**, 3619–3624.
- Westall J. C., Cernik M. and Borkovec M. (1998) Modeling metal speciation in aquatic systems. In *Metals in Surface Waters*, p. 191–216. Ann Arbor Press, Ann Arbor, MI.